OUKA
The University of Osaka
Institutional Knowledge Archive

Title	Development of rabbit VH with high affinity and improved stabilities
Author(s)	篠崎, 直也
Citation	大阪大学, 2018, 博士論文
Version Type	VoR
URL	https://doi.org/10.18910/70669
rights	
Note	

The University of Osaka Institutional Knowledge Archive : OUKA

https://ir.library.osaka-u.ac.jp/

The University of Osaka

DEVELOPMENT OF RABBIT VH WITH HIGH AFFINITY AND IMPROVED STABILITIES

Naoya Shinozaki

April 2018

Department of Biotechnology
Graduate School of Engineering
Osaka University

Table of Contents

Chapter 1

General Introduction

There are many unmet medical needs not yet satisfied in the world. In order to solve this, it is necessary to identify new disease-related molecules and discover the molecules that act on them, that is, pharmaceuticals. However, one modality (in this thesis, modality refers to the molecular type of therapeutic agent such as low molecular weight compounds and antibodies) is not always suitable to every disease-related molecules. To deliver innovative new drugs to patients suffering from diseases, we should continuously discover new modalities with different attractive features from conventional ones, and establish technologies that enable efficient pharmaceutical development with such new modalities.

1.1. The Rise of Biopharmaceuticals Centering on Pharmaceutical Antibodies

Low molecular weight compounds have played a central role in pharmaceuticals over the years. Sertürner F, a German pharmacist, succeeded to crystallize morphine in 1805 (Alston TA, 2017), and this was the first isolation of the active ingredient in nearly pure form from plant, and beginning of modern pharmaceutical science. From then, a large number of modern pharmaceuticals have been generated by extracting the active ingredients contained in plants, animals, minerals, etc., or by discovering compounds from artificially synthesized libraries. In 2000, all pharmaceuticals but one recombinant hematopoietic factor product (Epoetin alfa) were low molecular weight compounds in the top 10 sales ranking of world pharmaceutical market. Such a big success of low molecular weight compounds would be due to their various attractive features which are brought by chemically synthesized nature and small size generally less than 1000 Da; the potential to enter into inside the cells, the ability to control the activity of proteins (e.g. enzymes and channels) by entering their pockets, the chemical synthesizability in large amount, the availability of various administration route as patient-friendly oral administration.

The recent pharmaceutical industry has, however, undergone a major transformation period. Seven of the top 10 selling products became to be occupied by antibodies (Humira, Rituxan, Remicade, Avastin, and Herceptin) and other biopharmaceuticals (Enbrel, Lantus) in 2016 (Table 1). Regarding to low molecular weight compounds, while, only three products were in this ranking.

Table 1. World pharmaceutical sales ranking top 10 (2016)

Rank	Product name	Common Name	MW (~kDa)	Indication	Sales (million $)
1	Humira	Adalimumab	~150	RA/psoriasis etc.	16,078
2	Harvoni	Sofosbuvir + Ledipasvir	~1	Chronic hepatitis C	9,081
3	Enbrel	Etanercept	~150	RA/psoriasis etc.	8,874
4	Rituxan	Rituximab	~150	Non-Hodgkin's lymphoma	8,478[a]
5	Remicade	Infliximab	~150	RA/Crohn's disease etc.	8,234
6	Revlimid	Lenalidomide	~0.3	Multiple myeloma	6,974
7	Avastin	Bevacizumab	~150	Metastatic colon cancer	6,656[a]
8	Herceptin	Trastuzumab	~150	Breast cancer	6,655[a]
9	Lantus	Insulin glargine	~6	Diabetes	6,317[b]
10	Januvia	Sitagliptin	~0.4	Type 2 diabetes	6,109

Sales of each pharmaceuticals are cited from each manufacturer's annual report and biopharmaceutical products are shown on a light orange background. (a): Calculated the exchange rate from the Swiss franc to the dollar at the end of 2016 as 1.0191, (b): Calculated the exchange rate from the dollar to the euro as 1.0542 at the end of 2016.

Namely, it could be said that a paradigm shift from low molecular weight compounds to biopharmaceuticals centering on antibodies obviously occurred during less than twenty years. Such a paradigm shift would have been triggered by the exhaustion of disease-related molecules suitable for the target of low molecular weight compounds through decades of extensive drug discovery. Targetability of molecules for low molecular weight compounds can be limited by relatively low target specificity (sometime broadly act among target families), difficulty in the inhibition of protein-protein interactions, low solubility to aqueous solution, and so on. Low target specificity is especially troublesome because it causes undesirable side effects by acting on non-target molecules. In these situation, the development of pharmaceuticals specialized to act on an only target molecule that are called "molecular-targeted drugs" began in 1990s, and researchers focused their attention to antibodies which have high target specificities.

1.2. The Features and History of Pharmaceutical Antibodies

Antibody is a modality which has opposite features to the low molecular weight compounds; the high target-specificity which can distinguish even the difference of a few

amino acids, the ability to inhibit protein-protein interactions due to the large body, and the long half-life in the body of generally two to four weeks especially for IgG-type antibodies (Mankarious S *et al*., 1988). It can be considered that these features made antibodies one of the major modalities as shown in Table 1. Among these features, the highly specific binding to antigens would be the most attractive feature, because it enables precise targeting to disease-related molecules and then lowering the risk for undesirable side-effects by off-targeting. In fact, the mechanisms of actions of a great deal of antibodies that have been developed in various disease areas are basically based on specific binding to antigens.

Now every researchers can have an opportunity to obtain antibodies which are specific to desired target molecules. Also, pharmaceutical antibodies have been developed by a large number of pharmaceutical companies and institutions around the world. These facts indicate that antibody is now an easily accessible and very attractive modality for generating pharmaceuticals. However, it took a long time for antibodies to be widely used as pharmaceuticals. Antibody is originally a natural protein contributing to biological defense in the body and initial pharmaceutical antibody is “an immunoglobulin formulation” purified from human plasma which has been mainly used for the treatment of infectious disease from middle 20th century. Monoclonal antibodies against disease-related molecules became to be obtained after Köhler and Milstein established the mouse monoclonal antibody production technology using hybridoma in 1975 (Köhler G *et al.*, 1975). In addition, Winter G and colleagues reported that phage-display method, where genotype (antibody gene) and phenotype (antibody protein) are physically linked, can be used for antibody acquisition in 1991 (Marks JD *et al.*, 1991). This technology enabled to construct a vast size of library (10^{10}~10^{11}) and to screen binders efficiently. While, clinical application of mouse-derived monoclonal antibodies was limited by immunogenicity. Injection of heterologous proteins often induce production of neutralizing antibodies which reduce half-life of injected proteins and/or trigger cellular immunity causing toxicity. Such an immunogenic problem for antibodies were overcome by the establishment of humanizaiton technologies of heterogeneous antibodies (Roguska MA *et al.*, 1994). Regarding to antibody production, it had been initially carried out using mouse individuals and this method was not very efficient. Establishment of a cell culture engineering method, in which antibody genes are transfected into mammalian cells such as CHO cells for antibody production, led to the practical application of pharmaceutical antibodies. Therefore, it can be said that constant technological innovation made antibodies easily accessible and very attractive modality.

1.3. The Current Situation of Conventional Antibodies

The antibodies in Table 1 have basically identical structure to naturally existing IgG-type antibodies in the body, even though these pharmaceutical antibodies may have some artificial modifications for humanization and/or affinity maturation. In this article, such pharmaceutical antibodies are referred as "the conventional antibodies". The main mechanisms of actions of conventional antibodies are either of ligand neutralization (inhibition of biological signals by trapping soluble molecules), antagonistic activity (inhibition of biological signals through binding to membrane receptors), or agonistic activity (induction of biological signals through binding to membrane receptors). In addition, conventional antibodies may have a cytotoxicity (effector activity) by crosslinking effector cells to target cells via Fc regions of IgG1 or IgG3 (Vidarsson G *et al.*, 2014). For example, Avastin in Table 1 inhibits angiogenesis through binding to soluble ligands (VEGF) and neutralizing its activity (Ferrara N *et al.*, 2004). Both Humira and Remicade neutralize biological activity of TNF-α, a cytokine involved in systemic inflammation (Toussirot E and Wendling D, 2004). The mechanism of action of Rituxan, anti-CD20 monoclonal antibody, is considered to induce apoptosis signaling and to cause cytotoxicity with effector cells (Weiner GJ, 2010). It is proposed that Herceptin exhibits medicinal efficacy by inhibiting HER2 signaling and enlisting effector cells to attack and kill targeting cells (Sliwkowski MX *et al.*, 1999). The fact that as many as total 50 conventional antibodies have been launched over the past 20 years indicates how much resources for pharmaceutical research and development had been concentrated to this modality.

Table 2 shows the number of conventional antibodies of the cancer region and the non-cancer region which are in the market or in the late-stage clinical trial in 2017.

Table 2. The number of conventional antibodies in the market and in the late-stage clinical trial

	Cancer	Non-Cancer
In the market	25	25
In the late-stage clinical trial	6	33

Summarized the data from the website of National Institute of Health Sciences Division of Biological Chemistry and Biologicals (http://www.nihs.go.jp/dbcb/mabs.html) and reference (Reichert JM, 2017).

There are now 25 conventional antibodies for cancer treatment in the market and the exactly same number of conventional antibodies are sold for non-cancer treatment. Remarkably, this is not the case in the late-stage clinical trial. In non-cancer region, 33

late-stage clinical trials for conventional antibodies are in progress. In contrast, there are only 6 late-stage clinical trials in cancer area. This large difference in the conventional antibodies in the late-stage clinical trial indicates that development of conventional antibodies in cancer region have become difficult. Although there are some newly developed conventional antibodies with breakthrough concepts such as immune checkpoint inhibitors (Abdin SM *et al.*, 2018), the modalities that can have more drastic antitumor activities may have been needed in cancer region.

1.4. The Emergence of Next-Generation Antibodies

Recently, many kinds of antibodies which possess different mechanisms of actions from conventional antibodies have been developed. Such new antibodies are collectively referred as "next-generation antibodies" and some of them have been already in the market (Table 3).

Table 3. The number of next-generation antibodies in the market

Cancer		Non-Cancer	
Full IgG antibody-based			
RI-labelled Antibody (~150 kDa)	3		
Fc-engineered Antibody (~ 150 kDa)	2		
ADC (~ 150 kDa)	3		
Bispecific antibody (~150 kDa)	1		
Antibody fragment-based			
Bispecific antibody (scFv, ~50 kDa)	1	Antibody fragment (Fab, ~50 kDa)	3

Summarized the data from the website of National Institute of Health Sciences Division of Biological Chemistry and Biologicals (http://www.nihs.go.jp/dbcb/mabs.html) and reference (Reichert JM, 2017). Numbers in parentheses indicates the number of new disease-related molecules which are not targeted by conventional antibodies in the market.

Each of the next-generation antibodies have some chemical and/or biological modifications to exhibit unique mechanisms of actions. For example, Fc-engineered antibodies have greatly enhanced effector activities by various modifications in the Fc region, modulating affinities to Fc receptors on the effector cells (Saxena A *et al.*, 2016). The ADCs are generated to deliver toxic compounds precisely to cancer cells by connecting antibodies to toxic compounds via chemical linkers (Polakis P, 2016). Bispecific antibodies, which are made from two different antibodies, can bind two

different antigens and one application is able to recruit cytotoxic T cells to tumor cells by simultaneous binding to antigens of both cells (Zhou SJ *et al.*, 2017). These next-generation antibodies are also called "armed antibodies" and exhibit extremely potent antitumor effects that conventional antibodies are difficult to have.

There are more and more next-generation antibodies which are in the clinical development (Table 4).

Table 4. The number of next-generation antibodies in the late-stage clinical trial

Cancer		Non-Cancer	
Full IgG antibody-based modalities			
RI-labelled Antibody (~ 150 kDa)	1	Bispecific antibody (~ 150 kDa)	1
Fc-engineered Antibody (~ 150 kDa)	3		
ADC (~ 150 kDa)	7		
Antibody for Vaccination (~ 150 kDa)	1		
Antibody fragment-based modalities			
Immunotoxin (Fv, ~64 kDa)	1	Antibody fragment (Fab, ~50 kDa)	1
Immunotoxin (scFv, ~70 kDa)	1	Antibody fragment (scFv, ~25 kDa)	1
Immunocytokine (scFv, ~90 kDa + ~130 kDa)	1	Antibody fragment (VHH, ~12 kDa)	1
Immunolyposome (scFv, MW is unknown)	1		

Summarized the data from the website of National Institute of Health Sciences Division of Biological Chemistry and Biologicals (http://www.nihs.go.jp/dbcb/mabs.html) and reference (Reichert JM, 2017). Numbers in parentheses indicates the number of new disease-related molecules which are not targeted by conventional antibodies in the market.

The number of next-generation antibodies in the market and in the clinical development are outstandingly high in cancer region (Tables 3 and 4). Such a emergence of next-generation antibodies in cancer region would have a relation to the fact that the number of conventional antibodies in cancer region is being sluggish (Table 2). Namely, at least in this region, it is considered that next paradigm shift where next-generation antibodies play pharmaceutical central role is now occurring.

1.5. About the Antibody Fragments

As shown in Tables 3 and 4, next-generation antibodies are classified into two types,

one based on general IgG-type antibodies and one generated from antibody fragments. The antibody fragments can be used as they are as next-generation antibodies, or as components for producing other kinds of next-generation antibodies such as bispecific antibodies, immunocytokines, and so on.

The antibody fragments are antibodies downsized by fragmentation, keeping high antigen-specific binding activities (Figure 1).

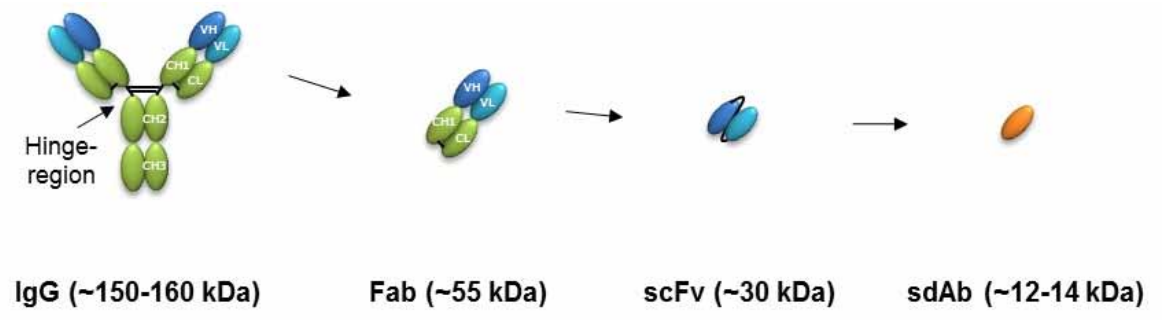

Figure 1. Schematic diagram of antibody fragments. Molecular weight of each antibody is cited from reference (Bannas P *et al.*, 2017). VH and VL are indicated in blue and light blue, respectively. The constant regions of heavy chain and of light chain are colored in green. Because sdAbs can be derived from some variable regions, they are collectively colored in orange.

IgG is almost 150 kDa of naturally existing immunoglobulin consisting of two heavy chains and two light chains. One heavy chain is composed of VH responsible for antigen-binding and three constant regions (CH1, CH2 and CH3), and one light chain is composed of VL responsible for antigen-binding and one constant region (CL). IgG is fragmented into two Fab' (Fab with a small portion of Fc) and Fc regions by digestion with papain. Fc region is consist of hinge-region and two CH2 and CH3 and relating to effector activities via binding to Fc receptors on the effector cells, and FcRn-dependent recycling which prolongs half-life in the body (Roopenian DC *et al.*, 2007). Fab is a domain on an antibody for antigen-binding, which is composed of one constant and one variable region of each of the heavy and the light chain. Its molecular weight is about 55 kDa that is almost one third of full length IgG. scFv is generated by linking one pair of variable regions (VH and VL) with flexible peptide linker which is usually composed of Gly and Ser. Its molecular size is 30 kDa, which is almost the half of Fab-type antibody. sdAbs are constituted by a single variable region and its molecular size is 12-14 kDa, which is almost the half of scFv and only one tenth of IgG-type antibodies.

Fragmentation gives antibodies several different biological properties from

conventional antibodies which has almost the same structural format as general IgG-type antibodies. First, antibody fragments have generally shorter half-lives than conventional antibodies. It is due to the faster renal elimination with their lowered molecular sizes below of renal clearance cutoff of ~50 kDa (Vaneycken I *et al.*, 2011), and the lack of FcRn-dependent recycling via Fc region (Roopenian DC *et al.*, 2007). This property can be advantageous in case that long-term circulation of antibody in the whole body cause undesirable side effects. In the clinical trial for wet-type AMD treatment with intravitreal injection, the occurrence rate of serious adverse events was higher with IgG-type Anti-VEGF antibody than Fab-type antibody for the same target (Martin DF *et al.*, 2012). Although interpretation of difference in the serious adverse events occurrence rate is uncertain, the short half-life might have been a key to avoid undesired side effects. Second, antibody fragments have high tissue penetration ability due to lowered molecular size. It is very important for drugs to reach the affected tissues where the disease-related target exists. There is a case that, when it administrated intravitreally, Fab-type antibody was diffused through the neural retina to the retinal pigment epithelial layer, although full length IgG-type antibodies did not penetrate the inner limiting membrane of the retina (Mordenti J *et al.*, 1999). Third, antibody fragments can be produced by not only mammalian cells but also microorganisms such as *E. coli.* and yeast. scFvs and sdAbs are especially suitable for phage display system, where a vast size of library can be produced by *E. coli.*, because of their low molecular weights and single strand natures. And finally, as antibody fragments have simplified architectures, it is easy to generate various next-generation antibodies by genetic fusion. Various types of bispecific antibodies can be easily produced by connecting two different fragment antibodies with flexible peptide linkers (Ulrich HW *et al.*, 2013). In contrast, it takes a lot of labor to generate bispecific antibodies which have the same structural format as IgG-type antibody (Lewis SM *et al.*, 2014). Other interesting application is immunocytokines in which fragment antibodies are genetically fused to cytokines with various biological activities. Many kinds of immunocytokines have ever been generated and clinically developed (Pasche N *et al.*, 2012).

1.6. The sdAb; The Smallest Antibody Fragment

sdAbs have the smallest and simplest architecture in the antibodies. These outstanding structural properties of sdAb may largely enhance the unique biological advantages of antibody fragments described in the previous section. There are various applications utilizing the unique properties of sdAbs (Figure 2).

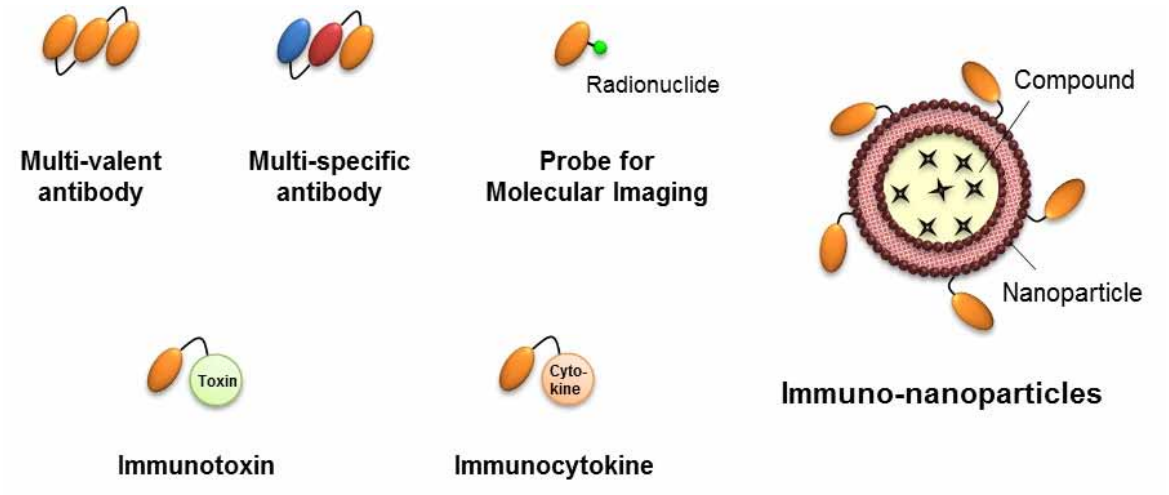

Figure 2. Various applications of sdAbs. sdAbs are indicated in orange ellipses. sdAbs which has different specificities from orange colored one are colored in red or blue.

First, multivalent and/or multispecific antibodies can easily be made by genetically connecting multiple sdAbs. For example, ALX-0171 is trivalent antibody generated from three Nb017 that is a monovalent sdAb to hRSV fusion glycoprotein (Palomo C *et al.*, 2016). Trivalent ALX-0171 showed about 6,000 to 10,000 times more potent biological activity than monovalent Nb017. As other example, ALX-0061 is bispecific antibody made from two different sdAbs which directed against IL-6R and HSA (Van Roy M *et al.*, 2015). ALX-0061 have a neutralization activity for soluble IL-6R and its plasma half-life can be extended by binding to HSA. As such, sdAb-derived multivalent and/or multispecific antibodies can have high functionality in the same or lesser molecular size than other antibody fragments. Second, sdAbs are considered to be an ideal probes especially for *in vivo* molecular imaging, where the high signal accumulation to affected tissues with minimal background is needed (Chakravarty R *et al.*, 2014). Molecular probes constituted by small sdAbs would achieve high tissue penetration and fast clearance from the body. Finally, a variety of sdAb-derived next-generation antibodies such as immunotoxins (Behdani M *et al.*, 2012; Li T *et al.*, 2016; Deng C *et al.*, 2017; Yu Y *et al.*, 2017), immunocytokines (Garcin G *et al.*, 2014), and immuno-nanoparticles (Heukers R *et al.*, 2014; Talelli M *et al.*, 2011; Talelli M *et al.*, 2013; van der Meel R *et al.*, 2012) have been generated.

1.6.1. The Problems on sdAb Obtainment

It is undoubtedly that sdAb is a promising modality, however, there may be rooms for

improvement on its generating sources. There are two types of sources for sdAbs; one is variable regions which usually constitute Fvs, and an another is naturally occurring single variable regions (Figure 3). The former source lacks high binding affinity, and latter is short of availability.

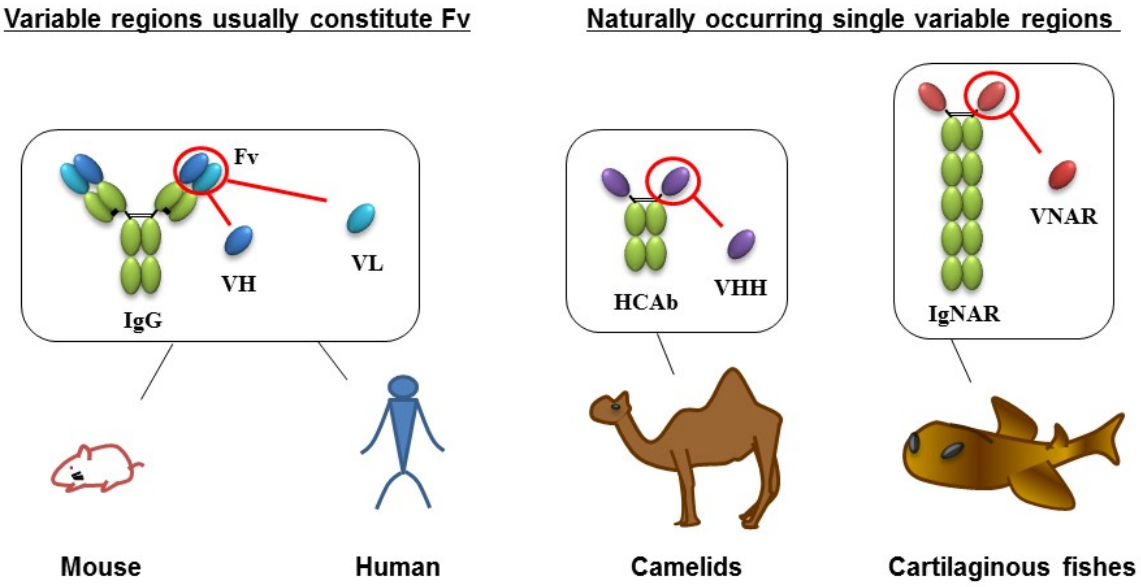

Figure 3. The possible source for sdAbs. Molecular weight of each antibody is cited from references (Bannas P *et al.*, 2017; Zielonka S *et al.*, 2015). VH, VL, VNAR, and VHH are indicated in blue, light blue, purple, and red respectively. The constant regions of heavy chain and of light chain are colored in green.

In 1989, Winter G and colleagues exhibited that VHs isolated from antibodies of immunized mice can have antigen-binding activities (Ward ES *et al.*, 1989). After that, many groups extensively studied about sdAbs derived of mouse and human variable regions (Jespers L, 2004; Holt LJ *et al.*, 2008; Hussack G *et al.*, 2012; Rouet R, 2015). Nevertheless, it is difficult to be said that these sdAbs are widely used for pharmaceutical research and development. One of the most important reasons for this would be their weak binding affinity; the K_D value is mostly several hundred nM to several μM, and at most tens of nM (Ward ES *et al.*, 1989; Jespers L, 2004; Holt LJ *et al.*, 2008; Hussack G *et al.*, 2012; Rouet R, 2015) In 1993, Hamers-Casterman and colleagues discovered that HCAbs, which are IgG-like antibodies devoid of light chains and CH1 domains, were abundantly present in the blood of camelids (Hamers-Casterman C *et al.*, 1993). The single variable regions of HCAbs, VHHs, can have strong binding affinities such as K_D

values of less than single-digit nanomolar, and are mainly used as a natural source for sdAbs. Some groups study cartilaginous fishes, which are known to produce IgNAR, an another heavy chain-only antibody, and single variable region of IgNAR (VNAR) also can be a source for sdAbs (Greenberg AS *et al.*, 1995; Zielonka S *et al.*, 2015). These natural single variable regions are certainly convenient for producing sdAbs, however, not every researchers can easily utilize such uncommon animals for immunization.

If such an inadequateness associated with the sources for sdAbs had been solved, sdAb-derived pharmaceutical antibodies could have dramatic progress. It is therefore highly desirable to discover other source of sdAbs, which can be widely used and have high antigen-binding abilities enough for therapeutic use. When high availability is required for the source of sdAbs, it is considered that usage of general antibodies in which two variable regions constitute Fv is more favorable. Such general antibodies that provide variable regions should possess very high affinities themselves, in order that single variable regions can have high affinities even after isolation. However, mouse antibodies are originally not expected to have high affinity, and human antibodies have ethical and technical difficulty in receiving *in vivo* affinity maturation. *In vitro* affinity maturation might improve the affinities of these sdAbs, though it is laborious and time-consuming and does not always succeed.

1.6.2. The Concern for Low Physical-Stability of Fv-Derived sdAb

Pharmaceutical antibodies should have a good physical-stabilities together with superior antigen-binding abilities. Physical-stabilities of proteins in solution are governed mainly by the combination of conformational stability that corresponds to the free energy difference between native and denatured states and colloidal stability that reflects the dispersion state of the protein molecules (Chi EY *et al.*, 2003; Uchiyama S, 2014). Decreases in conformational-stability and colloidal stability can promote aggregate formation during production, purification, and/or storage (Carpenter JF *et al.*, 2009; Uchiyama S, 2014), which is a potential cause of immunogenicity (Carpenter JF *et al.*, 2009).

Regarding to physical-stabilities, Fv-derived sdAbs may have rooms for improvement. The lack of partner variable region is presumed to cause reduction in the conformational-stability, because the difference in the free energy between scFv and unpaired VH was calculated to be 9.0 kJ/mol from the denaturation curve in the previous report (Röthlisberger D *et al.*, 2005). In addition, sdAbs isolated from Fv expose interacting interface between VH and VL, which is mainly consist of hydrophobic amino acid

residues, to solvent. The exposure of large hydrophobic surface could cause intermolecular interactions (Tamura T *et al.*, 2003) and thereby decrease the colloidal stability. Decrease in the colloidal stability leads the undesirable non-specific oligomerizations and eventually aggregations (Uchiyama S, 2014).

These reduction in physical stabilities of Fv-derived sdAbs should be cared both at the obtainment-step and after obtainment. In the case that single variable regions are directly used for obtainment step, it is necessary to pay attention so that valuable clones are not lost due to physical-instability. In addition, preparing the several approaches to improve physical-stabilities of obtained Fv-derived sdAbs is preferable to expand usability of obtained Fv-derived sdAb. One of the popular approaches to improve physical-stabilities would be the combination of random mutagenesis and phage-display system, however, it is laborious and time-consuming to create random libraries for every clone to find effective mutations. In addition, the resultant mutations in such approaches are sometimes involved at or near the CDRs (Arbabi-Ghahroudi M *et al.*, 2009; Perchiacca JM *et al.*, 2014), which are critical for antigen-binding abilities. It would be thus desirable to construct other methods to improve the physical-stabilities of Fv-derived sdAbs that have low risk of drastic reduction in the antigen-binding abilities and are universally applicable to various clones.

1.7. About the possibility of rabbit VH as sdAb

Rabbit is widely used animal for antibody obtainment as mouse is. It is well-known that antibodies produced by immunized rabbit are general IgG-type antibody and can have very higher affinity than those of mouse antibodies (Rossi S *et al.*, 2005; Borras L *et al.*, 2010; Landry JP *et al.*, 2015). The K_D values of IgG-type rabbit antibodies were shown to reach from tens of pM to hundreds of pM (Landry JP *et al.*, 2015). Based on our hypothesis that a single variable region of rabbit IgG-type antibody having very high affinity (e.g. K_D value in the pM order) can possess high affinity (e.g. K_D values of single-digit nM), even after isolated from Fv, the variable regions of rabbit was expected to be an ideal source of sdAbs with high affinity.

Comparing the variable regions of rabbit antibody, its VHs (rVHs) was considered to be more suitable as a source of sdAbs than its VLs (rVLs) from two reasons below. First, it was shown that rVHs tend to have longer CDR3s than rVLs (Kodangattil S *et al.*, 2014; Lavinder JJ *et al.*, 2014). The average amino acid length of CDR3 of rVLs was 12.0 ± 1.6 amino acids, while that of rVHs was 14.8 ± 3.6 amino acids (Lavinder JJ *et al.*, 2014). The longer CDR3 has possibility to create the wider surface area with larger

diversities which may enable to have higher specificity and binding affinity to target. Next, different from rVLs and VHs of other species, most of rVHs were found to have highly homologous framework regions (Borras L *et al.*, 2010; Kodangattil S *et al.*, 2014; Lavinder JJ *et al.*, 2014).Variable regions of antibodies are known to be encoded by *V*, *D*, and *J* (for VH), or *V* and *J* (for VL) of germ-line gene segments (Figure 4).

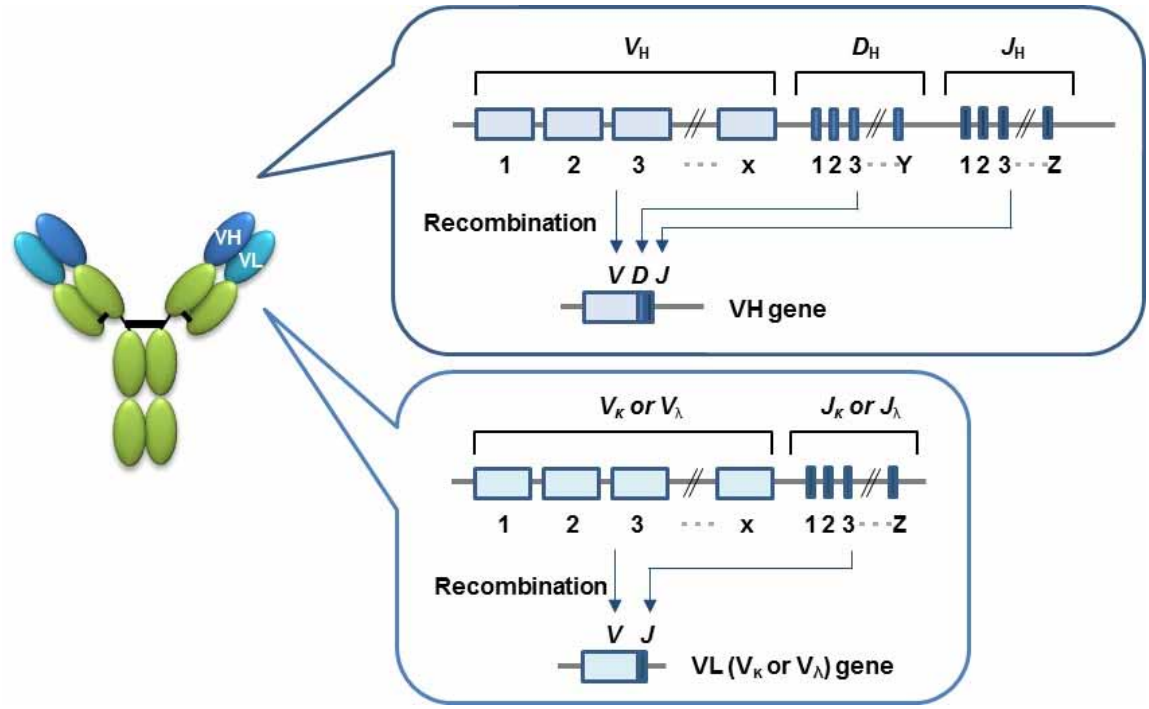

Figure 4. Recombination of genes encoding antibody variable regions. On somatic recombination, *V*, *D*, and *J* (for VH) or *V* and *J* (for VL) gene segments are selected from a large variety of germ-line gene segments to constitute genes of variable regions of IgG antibody.

In Figure 5, the regions of VH encoded by *V*, *D*, and *J* gene segment are indicated.

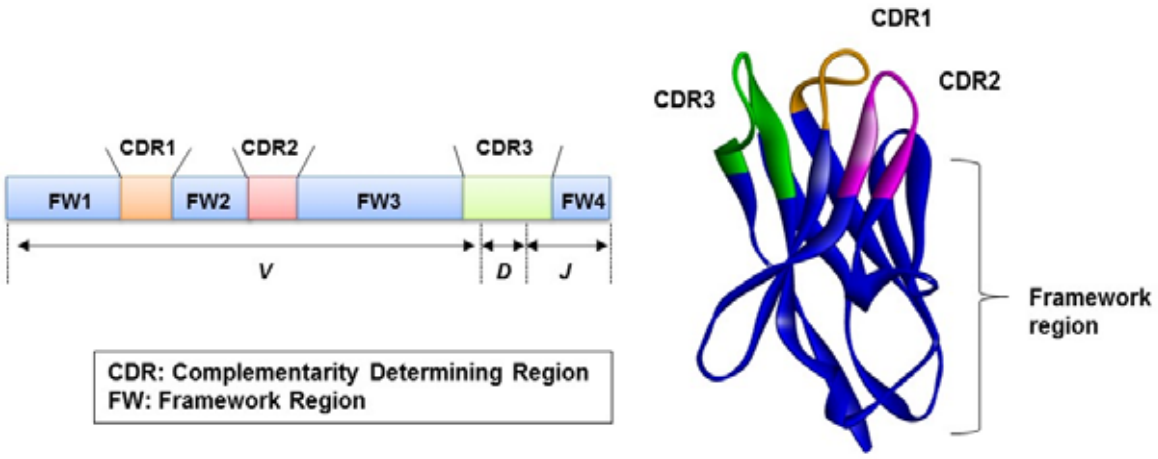

Figure 5. Schematic diagram of the primary structure (left) and three-dimensional structure (right) of VH. Under the primary structure, the regions encoded by *V*, *D*, and *J* segments are indicated by double-headed arrows.

V gene segment encodes from framework 1 to N-terminal of CDR3, *D* gene segment encodes intermediate of CDR3, and *J* gene segment encodes from C-terminal of CDR3 to framework 4. In the case of VL, *D* gene segment is absent. Here, rVHs are known to select very limited *V* and *J* gene segments on somatic recombination (Borras L *et al.*, 2010; Kodangattil S *et al.*, 2014; Lavinder JJ *et al.*, 2014) and this means most rVHs have highly homologous framework region because all framework regions are encoded by *V* and *J* gene segments (Figure 5). It is therefore expected that any rVHs have possibility to share various beneficial modifications in framework region due to having such an almost common framework region. In fact, Borras *et al.* reported that 15 different rabbit scFvs were successfully humanized by using common accepter framework (Borras L *et al.*, 2010).

1.8. Objective of This Thesis

By making it easier for more researchers to study sdAb, a promising next-generation antibody, it may be possible to create innovative new drugs that have never been seen before. The author considered that rVH, which have easy accessibility and the possibility of having high antigen-binding ability, might solve the problem on sdAb generation described above, however there were only a few reports for variable regions of rabbit (Suter M *et al.*, 1992). Thus we attempted to show rVHs as an highly available and usable source of sdAbs by achieving “Development of rVH with high affinity and

improved stabilities" in this thesis. The schematic-diagram of contents of this thesis is indicated in Figure 6.

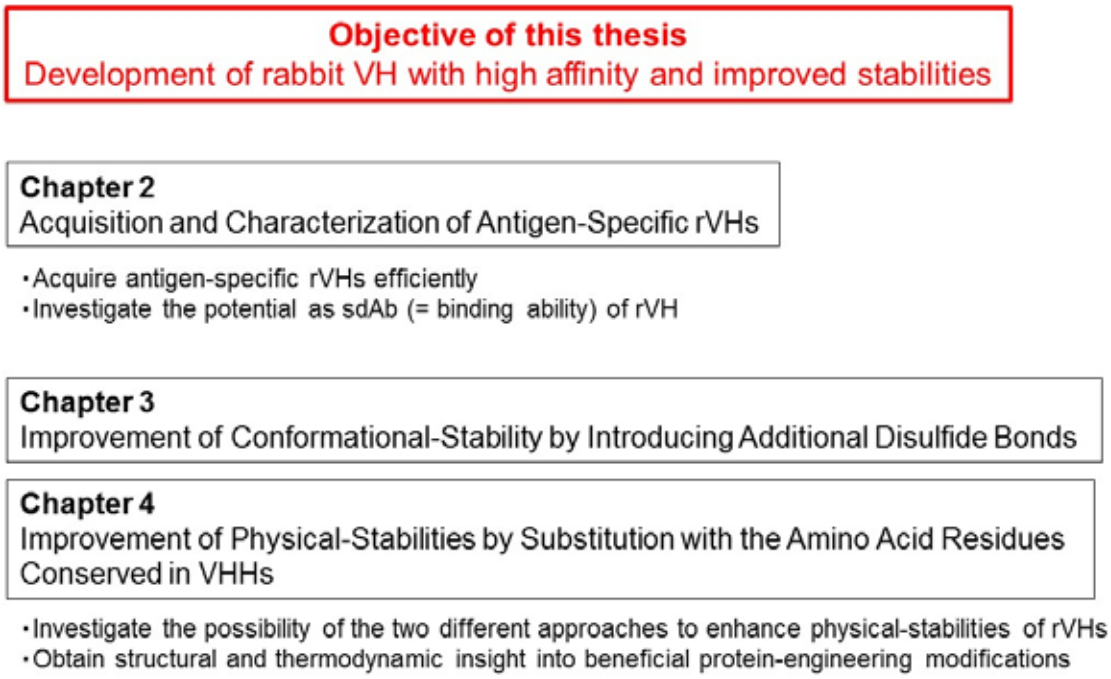

Figure 6. Schematic-diagram of contents of this thesis. The purpose of this thesis and the contents of the studies conducted for achieving the purpose in each chapter are shown.

First, antigen-specific rVHs were acquired from immunized rabbits and their physico-chemical properties including antigen-binding affinities were investigated (chapter 2). In acquiring, attempt was made to avoid the interruption caused by the instability of rVH due to rVL deficiency. Next, two different types of protein-engineering modifications were introduced to investigate their impact on the physical-stabilities of obtained rVHs (chapter 3 and 4). After that, structural and thermodynamic analysis were conducted to acquire the insight into physical-stabilizations by these modifications. Such information would be useful for further protein-engineering of sdAbs and other pharmaceutical proteins.

Chapter 2

Acquisition and Characterization of Antigen-Specific rVHs

In this chapter, antigen specific rVHs were obtained and characterized from immunized rabbits. Regarding to antibody acquisition, there are two general methods: a method using hybridomas (Köhler G *et al.*, 1975) and a method using phages (Marks JD *et al.*, 1991). The former method for rabbits has recently been reported (RabMAb® technology; covered by the following U.S. Patents, No. 5675063 and/or 7429487), however it is not very common. In addition, because binders are screened as general IgG-type antibodies in this method, rVHs may not have binding activities at all after isolation from obtained IgG binders. On the other hand, the strategy using phage display method shown in Figure 7 would enable to directly obtain antigen-binding rVHs, by displaying isolated rVHs on the phage.

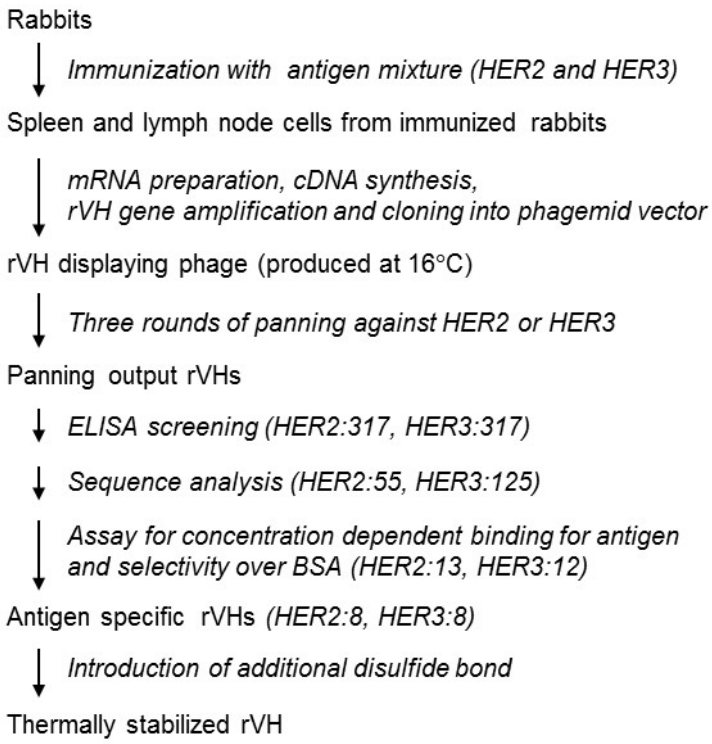

Figure 7. Flowchart outlining the procedure to obtain antigen specific rVHs.

As a procedure, rabbits are immunized with antigen at first, and their spleen and lymph node cells are obtained. In this thesis, HER2 and HER3 are used for immunization as representative cancer antigens. After extraction of extraction of mRNAs from these cells and cDNA synthesis, rVH genes are amplified by PCR. The phagemid vectors including rVH genes are used to transform *E. coli* and by culturing transformed *E. coli* the phage library displaying a variety of rVHs can be produced. After panning against each antigen, output clones are subjected to binder screening.

Upon displaying isolated rVHs on the phage, the author considered the stabilizing effect of the VH-VL interaction to rVH (Wörn A *et al.*, 1998; Jäger M & Plückthun A, 1999; Röthlisberger D *et al.*, 2005). rVHs separated from rVLs have to be displayed properly on the phage, even if such a stabilizing effect is actually lost. It was presumed that temperature at which phages are produced in *E. coli* was the key to achieving this. In the previous study, an attempt was made to obtain rVH binders using an rVH-displaying phage library produced at 25°C, resulted in obtainment of only weak binders (Suter M *et al.*, 1992). Even though this temperature is lower than 30°C or 37°C, generally used temperatures for rabbit scFv-displaying phages (Li Y *et al.*, 2000; Hawlisch H *et al.*, 2000; Makvandi-Nejad S *et al.*, 2010), proper display of rVHs on the phage could need further lower temperature than 25°C. Thus, in this chapter, the temperature was further lowered to investigate its impact on the rVH display level and obtainment of rVH binders.

2.1. Materials and Methods

2.1.1. Rabbit Immunization

Three Japanese white rabbits (Inoue-shouten, Takasaki-Shi, Gunma, Japan) were immunized with a mixture of 33 μg of recombinant human ErbB-2/HER2 protein (ACROBiosystems, Newark, DE, USA) and recombinant human ErbB-3/HER3 protein (ACROBiosystems) in combination with Freund's Complete Adjuvant. Seven days after the first immunization, rabbits were re-immunized with the same antigen mixture with Freund's Incomplete Adjuvant, and this process was repeated eight times every two weeks. Seven days after the final immunization, rabbits were euthanized to isolate spleen and lymph node cells. The serum titers of each antigen were checked by ELISA using HRP conjugated goat anti-Rabbit antibody (Immuno-Biological Laboratories Co., Ltd., IBL, Fujioka-Shi, Gunma, Japan) at seven days after the fourth, sixth and last immunization, respectively. All experiments with animals were approved by the

Institutional Animal Care and Use Committee of Daiichi Sankyo and carried out in strict accordance with the IBL guidelines for animal experiments, which complies with the laws concerning animal protection and management.

2.1.2. Preparation of rVH-Displaying Phage Library

From a total 1.9×10^8 spleen and lymph node cells of immunized rabbits, mRNAs were extracted using Dynabeads mRNA DIRECT Kit (Life Technologies Corporation, Grand Island, NY, USA) and reverse transcribed to cDNA with Transcriptor High Fidelity cDNA Synthesis Kit (Roche, Basel, Switzerland). Four 5'-sense and two 3'-antisense primers were designed to cover all rVH germ-line sequences and used for PCR to amplify rVH genes from the synthesized cDNA library. Amplified rVH genes were inserted into the Sfi I/Not I site of phagemid vector pCANTAB5E (Amersham plc, Buckinghamshire, UK) and fused following the 5' end of the E-tag (GAPVPYPDPLEPR) and the gIII coat protein of M13 bacteriophage (gIIIp) coding sequence. *E. coli* TG-1 strain (Agilent Technologies, La Jolla, CA, USA) was transformed with these phagemid vectors. Obtained transformants were pooled and infected with enough amounts of helper phage VCSM13 (multiplicity of infection > 100). Subsequently rVH displaying phages were produced by cultivation of these transformants at 16, 20, 22 or 25°C overnight with 2×YT medium supplemented with 0.25 mM IPTG, 100 μg/mL ampicillin, and 50 μg/mL kanamycin. Produced phage was then precipitated from overnight cultured medium using polyethylene glycol 6,000 and dissolved with PBS. Comparison of rVH display levels on the phage, 1.0×10^{10} virions of phages, produced at each temperature were subjected to WB using anti-E-tag antibody (Bethyl Laboratories, Montgomery, TX, USA), and appropriate secondary antibodies were used for detections. Virion numbers of purified phages were quantified using spectrophotometry with the following formula (Day LA & Wiseman RL, 1978).

$$\text{Number of virions / mL} = (A_{269} - A_{320}) \times 6 \times 10^{16} / (\text{number of nucleotide bases / virion})$$

Here, A_{269} and A_{320} indicate ultraviolet absorption of 269 and 320 nm, respectively, and the number of nucleotide bases per virion was set to be 5000.

2.1.3. Panning Against Antigens

The rVH displaying phage library was first subjected to negative selection using Dynabeads M-280 Streptavidin (Life Technologies Corporation) without antigen for

eliminating non-specific binders. All beads were previously blocked with BSA (Jackson ImmunoResearch Laboratories, Inc., West Grove, PA, USA) in all of the experiments. rVH-displaying phages unbound to the beads were then exposed to 50 pmol of biotinylated HER2 or HER3 at 4°C for overnight (first round) or at room temperature for one hour (second and third rounds). Biotinylated antigens were prepared using ChromaLink™ Biotin Antibody Labeling Kit (Solulink, Inc., San Diego, CA, USA) according to the manufacturer's instructions. Subsequently, new beads were added to recover biotinylated antigen binders. Library treated beads were washed by three different conditions as follows: PBS containing 3% (w/v) BSA and 0.05% Tween-20, PBS with 0.05% Tween-20, and PBS, respectively. Specific binders were eluted with 0.1 M Glycine-HCl (pH 2.2) and immediately neutralized with 1M Tris-HCl (pH 8.0). After that, *E. coli* TG-1 strain was infected with eluted phages and cultivated on an LB agar plate supplemented with 100 μg/mL of ampicillin. Appearing colonies were used for the next round of phage production or ELISA screening. For each round, phage titers were estimated from colony forming unit of input and output phages for *E. coli* TG-1 strain. Phage recovery rates of each round of panning were then calculated by Equation 1.

Phage recovery rate = Output phage titer / Input phage titer (1)

To confirm the concentration of antigen specific binders, panning without antigen was also conducted as a negative control at the third round.

2.1.4. ELISA Screening of Antigen-Binding rVHs

A randomly selected 317 output colonies from the third panning were inoculated to 2×YT medium supplemented with 100 μg/mL of ampicillin and 0.1% (w/v) glucose and cultivated at 37°C overnight. After final concentration of 0.5 mM, IPTG was added to induce rVH expression, and cultivation started again at 16°C. Lysozymes were then added to overnight culture and the mixture was transferred to a Nunc MaxiSorp flat-bottom 96-well plate (Thermo Fisher Scientific, Inc., Waltham, MA, USA) precoated with antigen (signal) or bovine serum albumin (noise). Bound rVHs were detected with HRP-conjugated anti-E-tag antibody (Bethyl laboratories) and > 2.0 as a signal-to-noise ratio was set as the criterion for positive. Positive clones with repeatability were regarded as a hit.

2.1.5. Preparation of rVHs

Genes encoding hit rVH clones were genetically linked with FLAG and His tag by PCR and inserted into pFLAG-CTS vector (Sigma-Aldrich, St. Louis, MO, USA) by homologous recombination. *E. coli* BL21 (DE3) strain (Merck Millipore, Darmstadt, Germany) was transformed with expression vector and obtained transformants were grown in LB medium supplemented with 100 μg/mL of ampicillin. When optical density at 600 nm reached to 1.0, rVH expression was induced by addition of IPTG at a final concentration of 1 mM and cultured at 16°C for overnight. Infected cell and culture medium was separated by centrifugation and collected cell pellets were subjected to osmotic shock with 20 mM Tris-HCl pH 8.0 supplemented with 0.5 M sucrose and 0.1 mM EDTA. The osmotic shocked supernatant was mixed with the cultured medium, and rVH was affinity purified from this mixture by using Ni Sepharose excel (GE Healthcare UK Ltd., Little Chalfont, Buckinghamshire, England). Concentration dependent ELISA were conducted using affinity purified rVHs, and as for VHs for evaluations of binding affinity and thermal stability, affinity purified rVHs were further purified with gel filtration using a Superdex 75 10/300 GL with AKTA system (GE Healthcare UK Ltd). rVH of the clone, H2-1-1, was prepared using an Expi293F mammalian cell expression system (Life Technologies Corporation) according to the manufacturer's instructions. The purities of finally purified rVH samples were confirmed by SDS-PAGE analysis and the protein concentrations were determined from the absorbance of 280 nm with the extinction coefficients which were calculated from amino acid sequences using Sednterp ver. 1.09 (University of New Hampshire, USA).

2.1.6. Physico-Chemical Analysis of rVHs

Binding activities of hit rVHs were evaluated by ELISA in triplicate at concentrations of 16, 125 and 1000 nM of affinity purified rVH with HRP conjugated anti-FLAG M2 antibody (Sigma-Aldrich). Those that showed apparent differences in intensities between antigen and BSA were regarded as antigen specific rVHs. Binding affinities were measured at 25°C by SPR using BIAcore T200 with a Series S Sensor Chip CM5 (GE Healthcare UK Ltd) coated directly with HER2 or indirectly by ErbB3 Fc Chimera (R&D Systems, Inc., Minneapolis, MN, USA) via Human Antibody Capture Kit (GE Healthcare UK Ltd). The kinetic parameters were determined by a 1:1 binding model of single cycle kinetics using BIAcore T200 Software.

To estimate the molecular state of rVHs, SEC-MALS analysis was conducted using a DAWN HELEOS II 8+ (Wyatt Technology Corp, USA, Santa Barbara, CA) with a Sepax Zenix-C SEC-300 column (Sepax Technologies, Inc., USA, Newark, DE).

To evaluate thermal stabilities, DSC was conducted using a MicroCal VP-Capillary DSC (Malvern Instruments Ltd, Worcestershire, UK.) at a heating rate of 60°C/h. The T_{peak} value (temperature where heat capacity takes the maximal value) was determined with rVH samples at a concentration of 0.2 mg/mL in PBS using the software MicroCal Origin 7 (Malvern).

2.1.7. Model Structure Construction and Structural Analysis

Model structures for obtained rVHs were constructed with the antibody structure prediction function of BioLuminate (Schrodinger, New York, NY). Structural analysis of VHH_{hCG} was conducted using available PDB data (PDB ID: 1HCV). The ASA of each residues were calculated using Discovery Studio Ver. 4.0 (Accelrys, San Diego, CA, USA). To estimate hydrophobicity of VL-interacting interfaces in obtained rVHs, ASA_{pol} and $ASA_{non\text{-}pol}$ of residues located at the VL-interacting interface were calculated using Discovery Studio Ver. 4.0. Here, ASA_{pol} is the ASA of polar components (N, carbonyl O, and OH) and $ASA_{non\text{-}pol}$ is ASA of non-polar components (aliphatic C, aromatic C, carbonyl C, and S) (Uchiyama S *et al.*, 2013) The residues of rVH in the VL-interacting interface were defined as the common residues, which are less than 5 Å from its VL, in the rVH of available rabbit Fv structures (PDB ID: 4HBC, 4HT1, 4JO1, 4JO4, 4O4Y). The ASAs of these rVHs, which were originally obtained as Fv (Arai H *et al.*, 2012; Pan R *et al.*,2013; Lammens A *et al.*, 2013; Malia TJ *et al.*, 2014), were also calculated with the three dimensional coordinates of the VH without the VL portion, which had been derived from the crystal structures of the Fv.

2.2. Results and Discussion

2.2.1. Production of rVH Displaying Phage

Rabbits were immunized with antigen mixture of HER2 and HER3 and confirmed the increased antibody titers for these antigens. A total of 1.9×10^8 spleen and lymph node cells of immunized rabbits were used to amplify rVH genes with primers designed to cover all germ-line genes of rVH (Table 5).

Table 5. Primers for amplification of rabbit VH genes

5’ sense primers
5’-TAACAATA GGCCCAGCCGGCC CAGTCGBTGGAGGAGTCCGG-3’
5’-TAACAATA GGCCCAGCCGGCC CAGTCRGTGAAGGAGTCCGAG-3’
5’-TAACAATA GGCCCAGCCGGCC CAGTCGSTGGAGGAGTCCAGG-3’
5’-TAACAATA GGCCCAGCCGGCC CAGGAGCAGCTGRWGGAGTCC-3’
3’ antisense primers
5’-TTTTCCTTTT GCGGCCGC TGAAGAGAYGGTGACSAGGG-3’
5’-TTTTCCTTTT GCGGCCGC TGARGAGACRGTGACCAGGG-3’

R = A or G, S = G or C, W = C or T, Y = C or T

A total of 8.0×10^8 transformants were obtained and it was expected that they covered most of the input rVH genes. For rVH-displayed phage production, the obtained transformants were first cultivated at several temperatures to investigate which temperature maximizes rVH display level. As a result, cultivation at 16°C gave the strongest band intensity corresponding to rVH-gIIIp fusion proteins, which are indicative of rVHs being displayed on the phage (Figure 8, upper band).

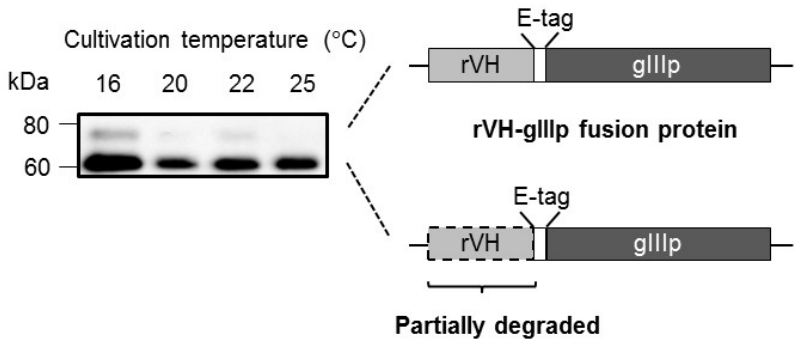

Figure 8. Display level of rVHs on the phage produced at various temperatures. The phages were produced at 16, 20, 22 and 25°C and subjected to WB (1.0×10^{10} virions per well). The rVH-gIIIp fusion protein was detected by anti-E-tag antibody and the amount of detected rVH-gIIIp fusion protein was correlated to the display level of rVHs. Fusion protein, which lacks an rVH portion, was also detected as a below band of the intact fusion protein.

The band became weaker as the cultivation temperature increased to 20 or 22°C and was

not detected at 25°C, which was used in the previous study (Suter M *et al.*, 1992). Thus, 16°C was adopted as the cultivation temperature to produce an rVH-displaying phage library. The lower bands shown in Figure 8 were considered to be impurities of rVH-gIIIp fusion proteins lacking the rVH region because their molecular weights (about 15 kDa) were consistent with the difference of molecular weight between the upper and lower bands. This consideration was supported by the fact that such an intense band was not observed for the control phage VCSM13 in Figure 9, which is composed of only native gIIIp.

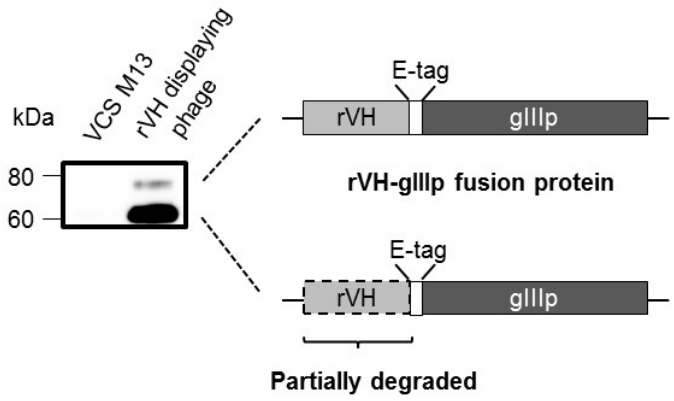

Figure 9. Detection of rVHs displayed on the phage. The rVH displaying phage produced at 16°C and control phage VCS M13 (composed of only tag-free native gIIIp) were subjected to WB (1.0×10^{10} virions per well). Detection of the rVH-gIIIp fusion protein was conducted with anti-E-tag antibody.

2.2.2. Acquisition of Antigen Specific rVHs

Starting from the prepared rVH phage library, phage recovery rates (numbers of output phage/input phage) increased step-wisely after every round of panning with each antigen (Figure 10). In the third round, remarkable differences in the phage recovery rates were confirmed between the panning with and without antigens. These results indicated that antigen-binding rVHs were concentrated from a vast number of library clones.

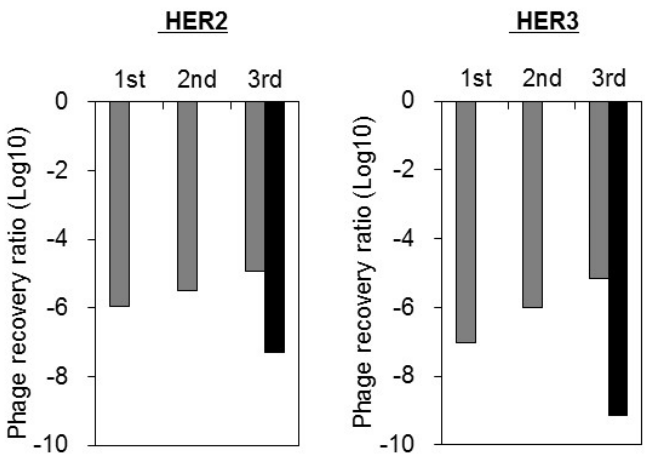

Figure 10. Phage recovery rates after panning against HER2 or HER3. Gray bars indicate phage recovery rates (ratio of output to input phage estimated as Materials and Methods) after each round of panning and black bars indicate phage recovery rates after the third round of panning without antigen.

After three rounds of panning, about 300 output clones were screened for their binding abilities to antigens by ELISA, and 55 and 125 hit clones were obtained for HER2 and HER3, respectively. These hit clones were subjected to sequence analysis and overlapped hit clones were eliminated. For both HER2 and HER3, eight rVHs of which amino acid sequences were indicated in Figure 11 were obtained respectively.

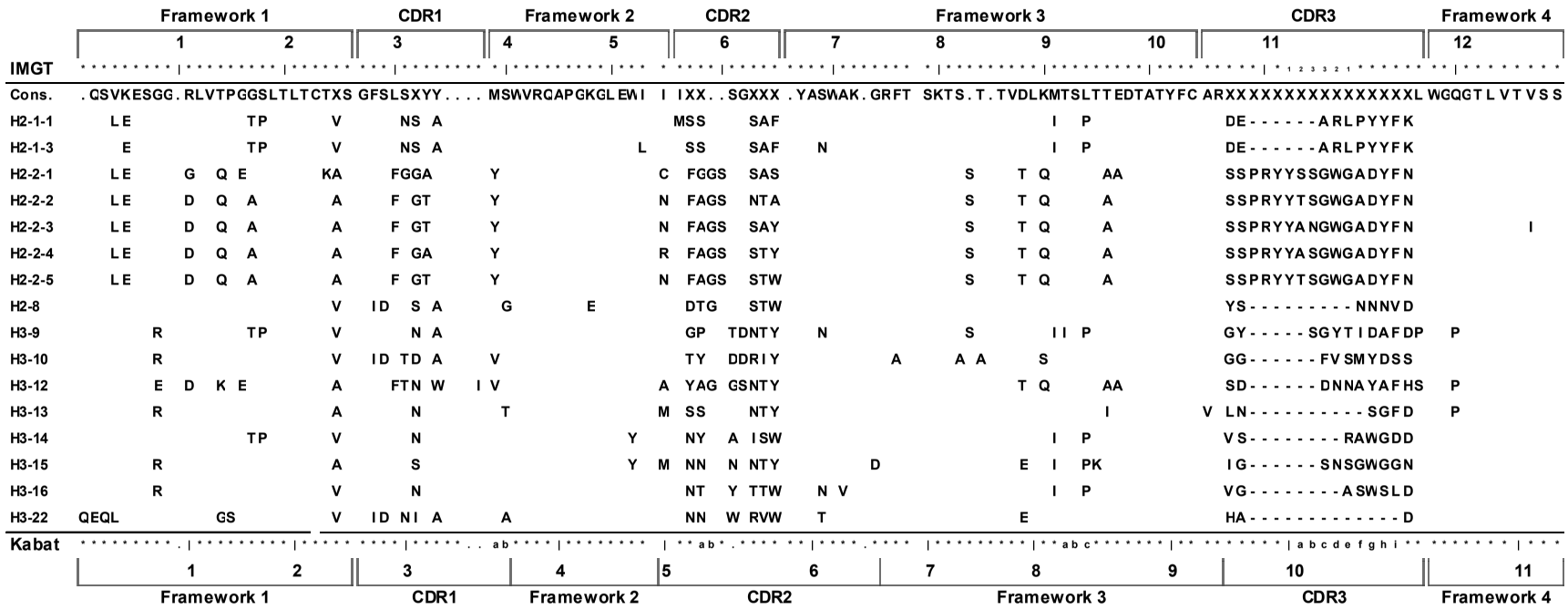

Figure 11. Amino acid sequences of the obtained 16 rVHs. Their consensus (Cons.) sequences are aligned according to IMGT (Lefranc MP, 1997) and Kabat (Kabat EA *et al.*, 1991) numbering. For each obtained rVH, only amino acids different from consensus sequences are indicated.

It was found that various rVHs with unique sequences were obtained. H2-1-1 and H2-1-2, or H2-2-1 to H2-2-5 were considered as family clones, respectively, because of their homology in the CDRs. These rVHs were assessed their concentration-dependent binding to antigens and non-specific binding to BSA (Figure 12).

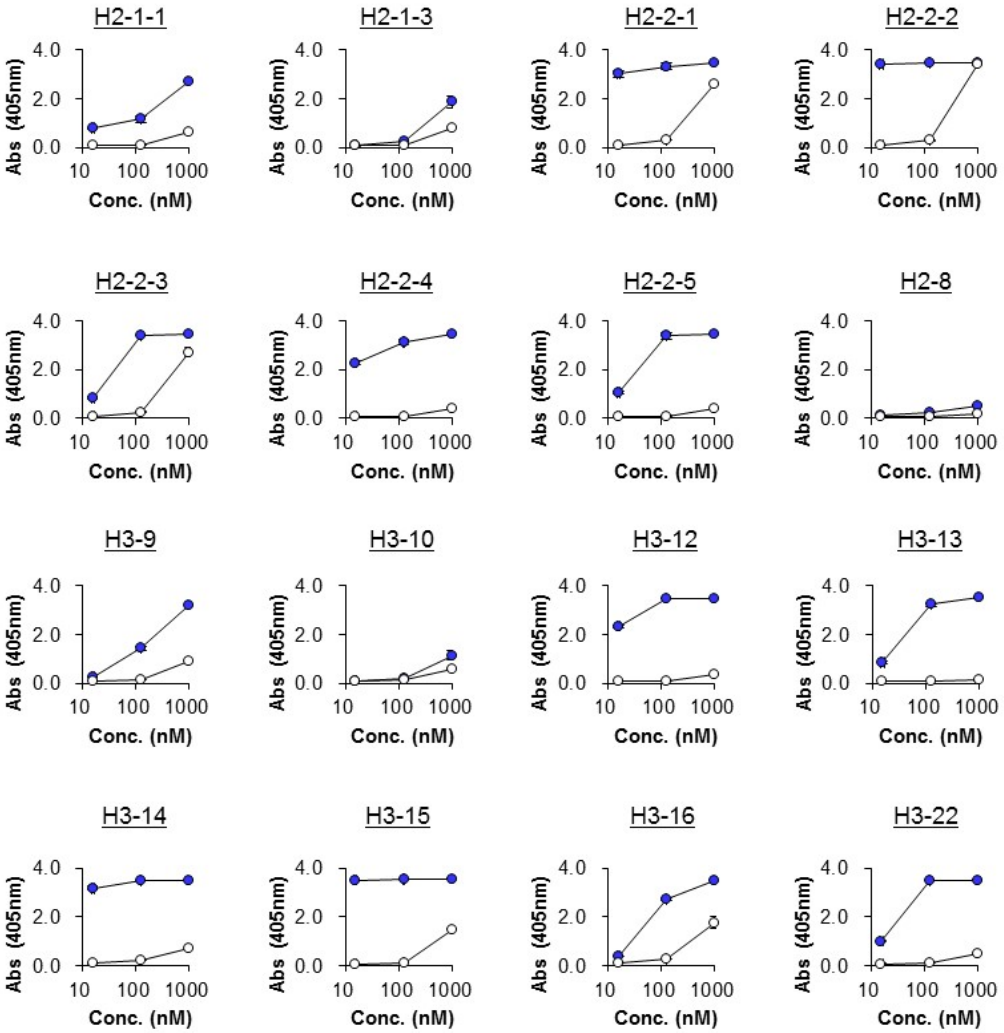

Figure 12. Dose-dependent ELISA binding assay of hit rVHs. Binding of hit rVHs to HER2 or HER3 (Blue) or BSA (white) were evaluated at concentrations of 16, 150 and 1000 nM. Data were collected in triplicate and standard deviation were indicated with the bars above and below of symbols.

All rVHs showed evident specific bindings to HER2 or HER3. It was expected from their strong ELISA signals that three HER2 specific binders, H2-2-1, H2-2-2, and H2-2-4, and three HER3 binders, H3-12, H3-14, and H3-15 have relatively high binding affinities.

2.2.3. Preparations of Obtained rVHs

5 hit clones were selected from 16 clones in Figure 12, which are two highly efficient ELISA binders (H2-2-2 and H3-15), moderate binder (H2-1-1) and two somewhat weak binders (H2-8 and H3-9), in order to investigate the relationship between ELISA results and dissociation constants from SPR. It was first tried to prepare these rVHs using *E. coli* and four rVHs except H2-1-1 could be obtained for enough amount to conduct physico-chemical analysis. The sample of H2-1-1 was prepared using mammalian cells. The purities of prepared rVHs were confirmed by the SDS-PAGE analysis (Figure 13).

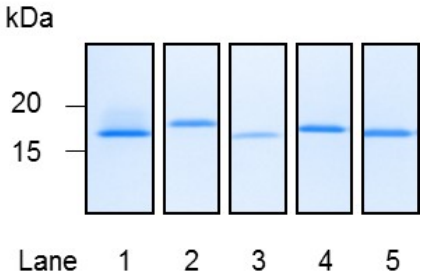

Figure 13. Confirmation of the purities of rVHs used for physicochemical analysis. About 2 μg of each purified proteins were loaded. Lanes 1-5 correspond to H2-1-1, H2-2-2, H2-8, H3-9, and H3-15.

After that, precise formation of endogenous disulfide (S-S) bond was confirmed for representative clones of H2-1-1, H3-9 and H3-15 by MS analysis after chymotrypsin digestion (Table 6).

Table 6. Peptides linked by S-S bond detected in MS analysis of representative rVHs

	Detected peptides linked by S-S bond		MW_{cal} (Da)	MW_{exp} (Da)
H2-1-1	(L) TLTCTVSGF (S)	(F) CARDEARLPY (Y)	2118.0	2118.0
	(L) TLTCTVSGF (S)	(Y) FCARDEARLPY (Y)	2265.1	2265.1
H3-9	(L) TCTVSGF (S)	(F) CARGY (S)	1279.5	1279.5
H3-15	(L) TCTASGF (S)	(F) CARIGSNSGW (G)	1732.7	1732.7

It was indicated by detection of expected peptides linked by S-S bond that purified rVHs with precise S-S bond have been prepared.

2.2.4. Physico-Chemical Characterizations of Obtained rVHs

Using purified samples in the previous section, obtained rVHs were characterized by several physico-chemical analysis. To evaluate binding abilities of obtained rVHs, kinetic parameters for antigen-binding were measured by SPR analysis. Regarding thermal stability, unfolding temperature (T_{peak}) was determined by DSC analysis. SEC-MALS analysis was conducted to investigate molecular state of rVHs. The results for these analyses are summarized in Table 7.

Table 7. Physico-chemical properties of obtained rVHs

	SPR			DSC	SEC-MALS	
	k_{on} ($M^{-1}s^{-1}$)	k_{off} (s^{-1})	K_D (nM)	T_{peak} (°C)	MW_{cal} (kDa)	MW_{exp} (kDa)
H2-1-1	7.3×10^4	1.6×10^{-3}	2.2×10^1	47.9	15.3	17.0 ± 0.7
H2-2-2	8.2×10^5	3.3×10^{-4}	0.4	37.7	16.0	18.9 ± 1.7
H2-8	ND	ND	3.9×10^2 *	80.2	14.9	13.3 ± 0.5
H3-9	ND	ND	1.9×10^2 *	66.9	15.5	13.9 ± 0.6
H3-15	2.6×10^6	2.0×10^{-3}	0.8	61.9	15.3	15.6 ± 1.2

ND: Not Determined

MW_{cal}: MW calculated from amino acid composition

MW_{exp}: Experimentally obtained MW

*K_D values were determined by steady–state affinity analysis, and k_{on} and k_{off} values were not obtained by this analysis.

As for binding affinity, H2-2-2 and H3-15 showed K_D values in a sub-nanomolar range; 0.4 nM for H2-2-2 and 0.8 nM for H3-15. K_D values of other rVHs (H2-1-1, H2-8 and H3-9) were in the range of from two to three-digit nM. Regarding thermal stability, H2-1-1 and H2-2-2 showed lower T_{peak} values (47.9 and 37.7 °C, respectively) than those of H2-8, H3-9 and H3-15 (80.2, 66.9 and 61.9 °C, respectively). In MS analysis, all rVHs were detected as the single peak around 15 kDa, indicative of monomeric and mono-disperse states for the rVHs. Taken together, it was found that rVHs can have high binding affinities, while, some of them were thermally unstable.

Here, T_{peak} value and the purification yield in the *E. coli* expression system of each rVH were plotted (Figure 14).

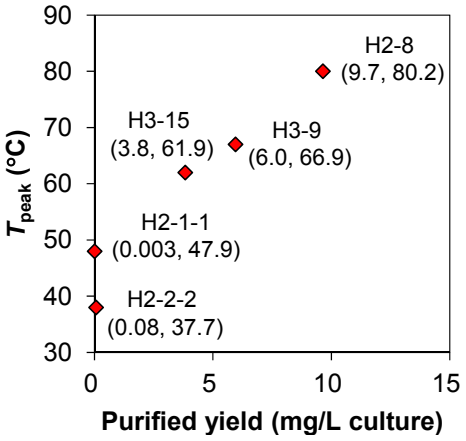

Figure 14. Plot of the purification yield of wild type rVHs with *E.coli* expression system vs respective T_{peak} value. Figures in parenthesis indicate purification yield (mg/L culture) with *E.coli* expression system and T_{peak} value (°C) of each rVH.

A good correlation was observed between T_{peak} values and the purification yields (R^2 = 0.94). Namely, rVHs which were more thermally stable had tendency to be produced more in *E. coli* expression system.

2.2.5. The Features of VL-Interacting Iinterface of Obtained rVHs

rVHs were obtained without their partner rVLs by displaying only rVHs on the phage. The features of VL-interacting interfaces of such rVHs were of interest and therefore compared with those of rVHs that had been previously obtained as Fv (Arai H *et al.*, 2012; Pan R *et al.*, 2013; Lammens A *et al.*, 2013; Malia TJ *et al.*, 2014). At first, model structures of five obtained rVHs were constructed using rabbit antibody structures that were available from PDB as a template (listed in Table 8).

Table 8. Component structures used to construct model structures of obtained rVHs

	Framework	CDR1	CDR2	CDR3
H2-1-1	4HBC	3IY6	2DTM	1MCP
H2-2-2	4JO3	3QNZ	3H0T	1DFB
H2-8	4HBC	3IY6	3IY1	3N85
H3-9	4HBC	2GJZ	2F5A	2VXV
H3-15	4HBC	1IFH	3STB	3IY3

The PDB IDs of component structures of rabbit antibodies used to construct model structures of obtained rVHs are indicated.

Using constructed model structures, the amino acid residues located on this interface were determined. The residues of rVHs in the VL-interacting interface were defined as the common residues, which were less than 5 Å from its VL, in the rVH of available rabbit Fv structures (PDB ID: 4HBC, 4HT1, 4JO1, 4JO4, 4O4Y). The amino acid residues on VH-VL-interacting interface of eleven rVHs obtained without rVL (H2-1-1, H2-2-2, H2-8, H3-9, H3-10, H3-12, H3-13, H3-14, H3-15, H3-16, and H3-22) and five rVHs obtained with rVL (4HBC, 4HT1, 4JO1, 4JO4, and 4O4Y) are indicated in Figure 15.

		FR2							CDR2	FR3	FR4	
		37	39	43	44	45	46	47	57	91	103	105
rVH	H2-1-1	**V**	**Q**	**K**	**G**	**L**	**E**	**W**	F	**F**	**W**	**Q**
	H2-2-2	**V**	**Q**	**K**	**G**	**L**	**E**	**W**	A	**F**	**W**	**Q**
	H2-8	**V**	**Q**	E	**G**	**L**	**E**	**W**	W	**F**	**W**	**Q**
	H3-9	**V**	**Q**	**K**	**G**	**L**	**E**	**W**	Y	**F**	**W**	P
	H3-15	**V**	**Q**	**K**	**G**	**L**	**E**	Y	Y	**F**	**W**	**Q**
	H3-10	**V**	**Q**	**K**	**G**	**L**	**E**	**W**	Y	**F**	**W**	**Q**
	H3-12	**V**	**Q**	**K**	**G**	**L**	**E**	**W**	Y	**F**	**W**	P
	H3-13	**V**	**Q**	**K**	**G**	**L**	**E**	**W**	Y	**F**	**W**	P
	H3-14	**V**	**Q**	**K**	**G**	**L**	**E**	Y	W	**F**	**W**	**Q**
	H3-16	**V**	**Q**	**K**	**G**	**L**	**E**	**W**	W	**F**	**W**	**Q**
	H3-22	**V**	**Q**	**K**	**G**	**L**	**E**	**W**	W	**F**	**W**	**Q**
VHH	1HCV	**F**	**Q**	**K**	**E**	**R**	**E**	S	Y	T	**W**	**Q**
	1BZQ	**F**	**Q**	**K**	**E**	**R**	**E**	**G**	L	**Y**	**W**	**Q**
	1KXQ	**F**	**Q**	**K**	**E**	**R**	**E**	**G**	Y	**Y**	**W**	**Q**
	1OP9	**F**	**Q**	**K**	**E**	**R**	**E**	**G**	Y	**Y**	**W**	**Q**
	1QD0	**F**	**Q**	**K**	**E**	**R**	**E**	F	W	**Y**	**W**	**Q**
	1ZMY	**F**	**Q**	G	**E**	**R**	**E**	A	Y	**Y**	**W**	**Q**
	1MEL	**F**	**Q**	**K**	**E**	**R**	**E**	**G**	Y	**Y**	**W**	**Q**

Figure 15. Amino acids of residues in the VL-interacting interface of rVHs. Residues are numbered according to Kabat numbering (Kabat EA *et al.*, 1991). Amino acid residues which are conserved in rVHs are indicated in bold characters. Amino acids of characteristic 105th residue are indicated in italic.

It was found that all amino acid residues except for 57th and 105th were highly conserved in rVHs. Amino acids at 57th residue in CDR2 were not unified, but tended to adopt hydrophobic ones. Amino acids at 105th residue were classified into two patterns of Gln or Pro. Eight rVHs out of eleven rVHs obtained without rVLs had Gln at 105th residue, on the other hand, all rVHs obtained with rVLs had Pro at the same position.

Next, hydrophobicity was compared for VL-interacting interfaces of rVHs. The $ASA_{non\text{-}pol}$s and ASA_{pol}s were calculated for rVHs obtained in this thesis and those from Fvs (Figure 16).

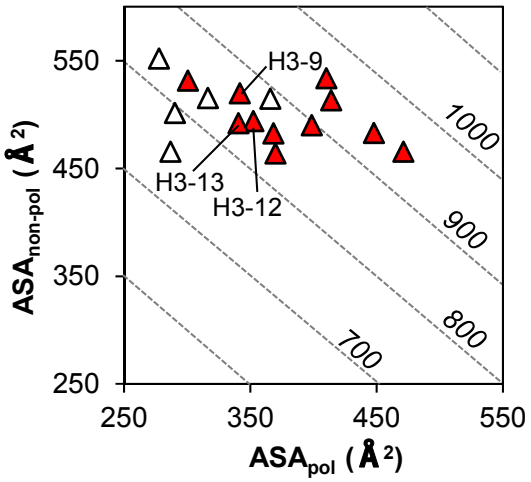

Figure 16. The plot of ASA_{pol} and $ASA_{non-pol}$ for respective rVHs. rVHs obtained in this thesis are indicated in red triangle and rVHs previously obtained as Fv (Arai H *et al.*, 2012; Pan R *et al.*,2013; Lammens A *et al.*, 2013; Malia TJ *et al.*, 2014) are indicated in open triangle. The dashed lines indicate the area where the sum of ASA_{pol} and $ASA_{non-pol}$ is the same, and the value of total ASA are indicated above the dashed lines.

Because average $ASA_{non-pol}$s were 497 ± 24 Å^2 for rVHs obtained without rVLs and 510 ± 31 Å^2 for rVH obtained with rVLs (Figure 16), it could be said that no difference was found between their $ASA_{non-pol}$. On the other hand, the average ASA_{pol}s of 383 ± 51 Å^2 for rVHs obtained without rVLs and of 307 ± 36 Å^2 for rVH obtained with rVLs (Figure 17) indicate a tendency of larger ASA_{pol} of rVHs obtained without rVLs.

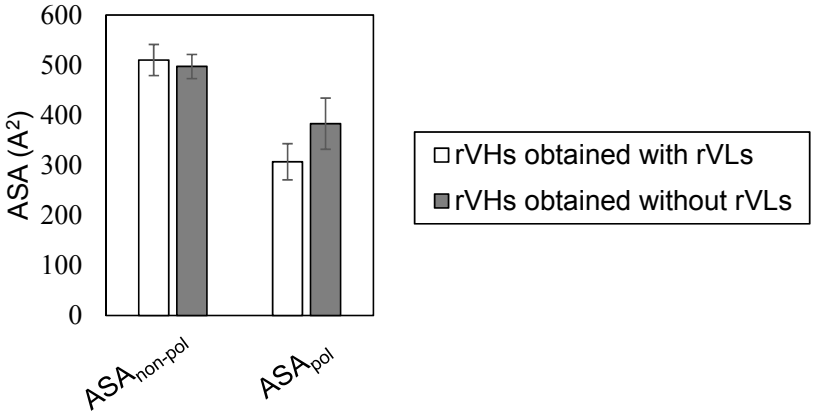

Figure 17. The average ASA_{pol} and $ASA_{non-pol}$ of rVHs obtained with and without rVLs

These results might originate from the elimination of rVHs with hydrophobic VL-interacting interfaces during the panning step using hydrophobic magnetic beads and microtubes.

Figure 15 showed that there is a difference in the adopt of amino acid at 105th residue between rVHs obtained in this thesis and those from Fvs. Therefore, $ASA_{non\text{-}pol}$ and ASA_{pol} were calculated for 105th residue of each rVHs (Figure 18).

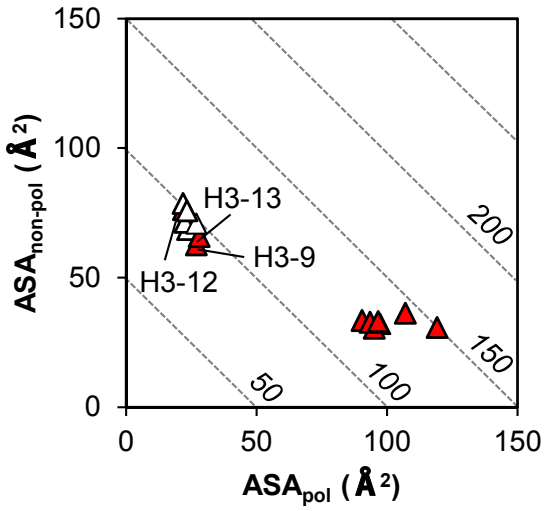

Figure 18. The plot of ASA_{pol} and $ASA_{non\text{-}pol}$ for residue 105 of respective rVHs. rVHs obtained in this thesis are indicated in red triangle and rVHs previously obtained as Fv (Arai H *et al.*, 2012; Pan R *et al.*,2013; Lammens A *et al.*, 2013; Malia TJ *et al.*, 2014) are indicated in open triangle. The dashed lines indicate the area where the sum of ASA_{pol} and $ASA_{non\text{-}pol}$ is the same, and the value of total ASA are indicated above the dashed lines.

Compared with the Pro at residue 105, Gln had a smaller $ASA_{non\text{-}pol}$ (30 $Å^2$–40 $Å^2$ smaller) and larger ASA_{pol} (80 $Å^2$–100 $Å^2$ larger), providing a higher hydrophilic surface area at the VL-interacting interface of rVHs obtained without rVLs. Considering that the VHHs, which are a natural single domain variable region of camelids, also adopt Gln (Hagihara Y *et al.*, 2007; Saerens D *et al.*, 2008; Hussack G *et al.*, 2011), Gln at the residue 105 of sdAbs might generally be advantageous from the point of colloidal stability. Further investigation of colloidal stabilities, three-dimensional structures of rVHs, and their molecular states in highly concentrated solution (Ota C *et al.*, 2016) will clarify the general rules of VH stabilization.

2.3. Summary of This Chapter

In this chapter, rVHs were shown to have the potential for specific binding to antigens with sub-nanomolar K_D values. Based on our knowledge, this is the first report to obtain such high affinity binders composed of an unpaired variable region (Ward ES *et al.*, 1989; Jespers L, 2004; Holt LJ *et al.*, 2008; Hussack G *et al.*, 2012; Rouet R, 2015). As correlation was observed for representative five rVHs between binding activity of ELISA (Figure 12) and dissociation constants of SPR (Table 7), other rVHs which showed strong binding activity of ELISA, such as H2-2-1 or H3-14, were expected to have similar high affinity as those of H2-2-2 and H3-15.

Upon acquisition of the rVHs, their reduction in conformational stabilities was presumed because they lack partner VLs (Wörn A *et al.*, 1998; Jäger M & Plückthun A, 1999; Röthlisberger D *et al.*, 2005). Such presumption elicited our concern that phage production at high temperatures might cause inefficient display of rVHs on the phage. It was attempted to dispel this concern by producing phage library at lowered temperature. As a result, rVH display level was enhanced and a variety of HER2 and HER3 binders were obtained. The fact that some of obtained rVHs were poorly produced in *E. coli* and thermally unstable (Figure 14) suggests that lowered temperature, which was expected to enhance soluble expression and/or suppress thermal unfolding (Correa A & Oppezzo P, 2015), was the key to achieve binder acquisition.

Chapter 3

Improvement of Conformational-Stability by Introducing Additional Disulfide Bonds

In this chapter, the method was constructed to enhance thermal stabilities of rVHs by introduction of additional disulfide (S-S) bond. Other groups reported introduction of such S-S bond at the 54th and 78th residues (IMGT numbering) of camelid VHH (Hagihara Y *et al.*, 2007; Saerens D *et al.*, 2008; Hussack G *et al.*, 2011). Most of the VHHs were successfully stabilized by the S-S bond with relatively small negative effect on the binding affinity to the antigen, while some VHHs lost their antigen-binding abilities (Hussack G *et al.*, 2011). Therefore, it was thought to be intriguing to investigate the impact of this S-S bond on the thermal stabilities and affinities of rVHs, and to learn what kind of factors control them. The additional S-S bond was finally introduced into obtained rVHs and its impact on thermal stabilities and affinities was examined.

3.1. Materials and Methods

3.1.1. Model Structure Construction and Structural Analysis of S-S bond Introduced rVHs

To argue the possibility of additional S-S bond introduction to rVHs, model structures of rVHs with additional S-S bonds were created using the function of Discovery Studio Ver. 4.0. Structural analysis of VHH_{hCG} was conducted using available PDB data (PDB ID: 1HCV). The ASA of residues for Cys mutation and estimated RMSD of Cα of residues in the framework were calculated using Discovery Studio Ver. 4.0.

3.1.2. Introduction of Additional S-S Bonds to rVHs

For additional S-S bond introduction, Gly or Ala and Ile at positions 54 and 78 of rVHs were both mutated to Cys by site-directed mutagenesis. Cys introduced mutants were prepared by the same methods as wild type rVHs, and S-S bond formations were confirmed for H2-1-1, H3-9, and H3-15 as wild type.

3.1.3. Thermodynamic Analysis of rVHs

To obtain detailed thermodynamic parameters, DSC analysis was conducted at 1.0

mg/mL using a MicroCal VP-Capillary DSC. The ΔH values were estimated by the integration of endothermic heat accompanied by the unfolding. The T_m values were determined as the temperature at which the integration of endothermic heat is equal to half the area of ΔH. The enthalpy change ($\Delta H(T)$), entropy change ($\Delta S(T)$) and free energy change ($\Delta G(T)$) are indicated as Equations 2-4.

$$\Delta H(T) = \Delta H + \Delta C_P(T - T_m) \quad (2)$$

$$\Delta S(T) = \Delta S + \Delta C_P \ln(T/T_m) \quad (3)$$

$$\Delta G(T) = \Delta H(T) - T\Delta S(T) \quad (4)$$

From Equations 2-4, ΔS can be calculated as $\Delta H/T_m$ because ΔG becomes zero at T_m. In this analysis, the author assumed that ΔC_P was constant and determined as the difference between the baseline of folded and unfolded states in the DSC curve.

3.2. Results and Discussion

3.2.1. Structural Validity of Additional S-S Bond Introduction into rVHs

Prior to the actual S-S bond introduction into rVH, the structural validity of this method was verified. Because Cys is a hydrophobic amino acid, the residues of Cys mutations should be buried in a structure so as not to alter the hydrophobicity of the structure's surface. In fact, ASAs of residues mutated to Cys were less than 20% in the previous studies that reported the introduction of artificial S-S bonds into subtilisin BPN' (Mitchinson C & Wells JA, 1989), *B. circulans* xylanase (Wakarchuk WW *et al.*, 1994), AprP (Ko JH *et al.*, 1996), human carbonic anhydrase II (Burton RE *et al.*, 2000; Mårtensson LG *et al.*, 2002), manganese peroxidase (Reading NS & Aust SD, 2000). Therefore, it calculated ASAs of 54th and 78th residues using five model structures of rVHs constructed in previous chapter (Table 9).

Table 9. The calculated ASA (%) of residues for Cys replacement

	H2-1-1	H2-2-2	H2-8	H3-9	H3-15
G/A54	0	0	0	0	0
I79	7.4	5.0	8.6	8.6	8.6

The calculated ASAs of the model structures were less than 10%, indicating that these

residues were buried deep inside in the model structures.

Next, in order to investigate if the S-S bond between C54 and C78 (C54-C78) would invoke structural alteration, the RMSDs (Å) were calculated between rVHs with C54-C78 and without C54-C78 using model structures (Table 10).

Table 10. The calculated Cα RMSDs (Å) of rVHs and VHH_{hCG}

H2-1-1	H2-2-2	H2-8	H3-9	H3-15	VHH_{hCG}
0.3	0.2	0.3	0.3	0.4	0.3

The Cα RMSDs of the five rVHs showed values similar to that of VHH compared to the α-subunit of human chorionic gonadotropin (VHH_{hCG}, PBD ID: 1HCV). Because VHH_{hCG} was successfully thermally stabilized by C54-C78 without loss of binding affinity (Hagihara Y *et al.*, 2007), the introduction of C54-C78 was unlikely to have a negative impact on the rVHs' binding affinities to antigens.

Based on these considerations, the attempt was made to introduce an additional S-S bond into the wild type rVHs by Cys mutation of 54th and 78th residues.

3.2.2. Preparation and Physico-chemical Characterization of Additional S-S Bond Introduced rVHs

The rVHs whose 54th and 78th residues were mutated to Cys (C54-C78 mutant) were prepared by the same method as wild type rVHs and those purities were confirmed by SDS-PAGE analysis (Figure 19).

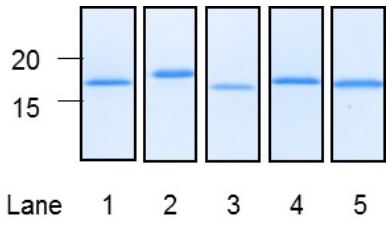

Figure 19. Confirmation of the purities of C54-C78 mutant rVHs used for physicochemical analysis. About 2 μg of each purified proteins were loaded. Lanes 1-5 correspond to C54-C78 mutant of H2-1-1, H2-2-2, H2-8, H3-9, and H3-15.

It was not clearly observed that purification yields were improved by S-S bond introduction under preparation conditions of this thesis using *E. coli*. While, in the case

of H2-1-1 which was prepared using mammalian cell, purification yield of its C54-C78 mutant was increased to 3- or 7-fold compared with wild type.

The formation of C54-C78 was experimentally confirmed for representative C54-C78 mutants by MS analysis after chymotrypsin digestion (Table 11).

Table 11. Peptides linked by S-S bond detected in MS analysis of C54-C78 mutants

	Detected peptides linked by S-S bond		MW_{cal} (Da)	MW_{exp} (Da)
H2-1-1	(L) TLTCTVSGF (S)	(F) CARDEARLPY (Y)	2118.0	2118.0
	(L) TLTCTVSGF (S)	(Y) FCARDEARLPY (Y)	2265.1	2265.1
	(F) TCSKTSTTVDL (K)	(W) ICIM (S)	1630.8	1630.8
H3-9	(L) TCTVSGF (S)	(F) CARGY (S)	1279.5	1279.5
	(W) ICIIGPTDNTY (Y)	(F) TCSKTSSTTVDL (K)	2448.1	2448.1
H3-15	(L) TCTASGF (S)	(F) CARIGSNSGW (G)	1732.7	1732.7
	(Y) ICM (I)	(F) TCSKTSTTVEL (K)	1531.7	1531.7

Chymotrypsin digestion of rVH mutants produced peptide fragments linked with C54-C78 or C23-C104 as expected. Neither undesired peptide fragments linked with other combinations of S-S bond nor those with free Cys were detected. These results indicated that both of the two S-S bonds were correctly formed as designed.

Using C54-C78 mutant samples purified in the previous section, antigen-binding activities and thermal stabilities were evaluated by SPR and DSC. The results are summarized in Table 12.

Table 12. Kinetic parameters for binding of C54-C78 mutants to each target in SPR analysis

	SPR			DSC	
	k_{on} ($M^{-1}s^{-1}$)	k_{off} (s^{-1})	K_D (nM)	T_{peak} (°C)	ΔT_{peak} (°C)
H2-1-1	1.5×10^5	1.4×10^{-2}	9.2×10^1	78.2	30.3
H2-2-2	6.1×10^5	1.6×10^{-3}	2.7	60.4	22.7
H2-8	ND	ND	8.7×10^{2} *	100.8	20.6
H3-9	ND	ND	$> 5.0 \times 10^{3}$ *	90.3	23.4
H3-15	1.2×10^6	2.5×10^{-3}	2.0	81.8	19.9

ND: Not Determined

*K_D values were determined by steady–state affinity analysis, and k_{on} and k_{off} values were not obtained by this analysis. K_D value for the C54-C78 mutant of H3-9 could not be determined up to 5 μM.

It was shown that the K_D values of each mutants was within several-fold of respective wild type counterparts (Table 12), except for H3-9. The T_{peak} values of all mutants were more than 20°C higher than those of corresponding wild type rVHs (Table 12). Taken together, rVHs can be highly thermally stabilized by C54-C78 introduction without severe loss of binding affinities.

It is noteworthy that increase in the unfolding temperature by introduction of C54-C78 were much larger for rVHs in this thesis than that for VHHs in previous reports (Figure 20).

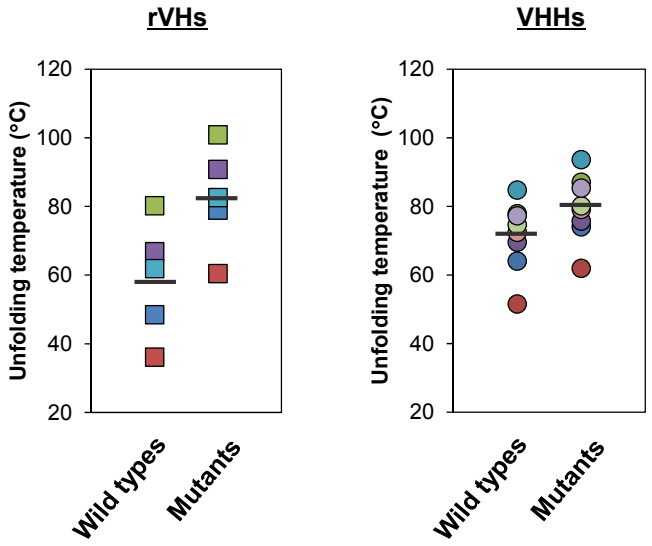

Figure 20. Comparison of increase in the unfolding temperature of rVHs and VHHs due to C54-C78 introduction. Unfolding temperature of wild types and their corresponding C54-C78 mutants are indicated as the same symbol and color for rVH and VHH. Average thermal unfolding temperatures of each group are indicated with bold lines. The unfolding temperatures of VHHs were quoted from references (Hagihara Y *et al.*, 2007; Saerens D *et al.*, 2008; Hussack G *et al.*, 2011).

The shift of unfolding temperature was 24.0°C for rVHs and 9.0°C for VHHs on average (average unfolding temperature of rVHs, mutant rVHs, VHHs, and mutant VHHs were 58.7°C, 82.7°C, 71.9°C, and 80.9°C, respectively).

3.2.3. Thermodynamic Analysis of C54-C78 Mutant rVHs

It is intriguing to investigate the major factors that contributed to such high thermal stabilization of rVHs. Therefore, the thermodynamic parameters and T_m, at which the Gibbs free energy change (ΔG) becomes zero, were determined for H2-2-2 and its C54-C78 mutant by DSC analysis. In comparison, those of VHH_{hCG} were estimated based on the published data (Hagihara Y *et al.*, 2007). Their thermal unfolding curves for H2-2-2 and its C54-C78 mutant are shown in Figure 21.

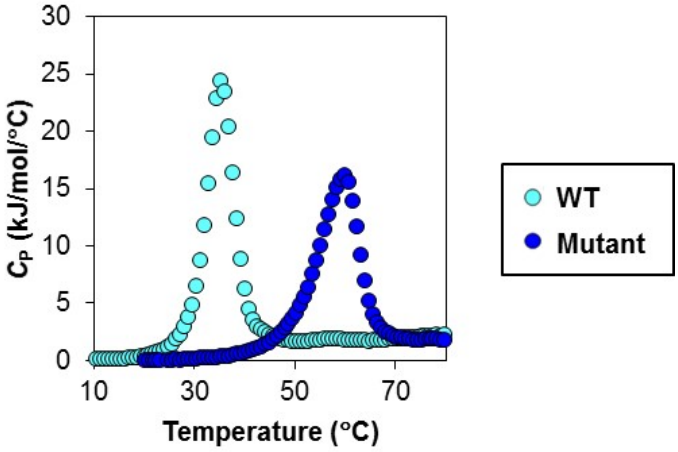

Figure 21. The thermal unfolding curve of H2-2-2 (light blue) and its C54-C78 mutant (blue) in the DSC analysis.

Thermodynamic parameters are obtained from thermal unfolding curves and indicated in Table 13.

Table 13. Thermodynamic parameters of H2-2-2 ahd VHH_{hCG}

		T_m (°C)	ΔH (kJ/mol)	ΔS (kJ/mol/K)	ΔC_P (kJ/mol/K)
H2-2-2	WT	35.1	161.4 ± 1.9	532.8 ± 6.0	1.5 ± 0.1
	Mutant	58.1	158.6 ± 3.2	478.8 ± 9.6	1.7 ± 0.1
VHH_{hCG}	WT	46.0	346.8 ± 5.4	1086.6 ± 16.9	4.8 ± 0.4
	Mutant	56.0	369.2 ± 9.4	1121.7 ± 28.6	5.2 ± 0.4

For VHH_{hCG}, T_m and ΔC_P were quoted from reference (Hagihara Y *et al.*, 2007) and other thermodynamic parameters were calculated using published data of the same reference.

As for T_m, the T_m increase (ΔT_m) of H2-2-2 was more than 20°C (from 35.0°C to

58.1°C), while that of VHH_{hCG} was 10°C (from 46.0°C to 56.0°C). Regarding the enthalpy and entropy change accompanied by the thermal unfolding (ΔH and ΔS), the mutant of H2-2-2 showed the values of 158.6 kJ/mol and 478.8 J/mol/K, respectively. These values were less than half those of mutant of VHH_{hCG} (369.2 kJ/mol and 1121.7 J/mol/K, respectively). In terms of the influence of the C54-C78 introduction on the ΔH and ΔS, compared to their wild types both ΔH and ΔS were slightly decreased for the mutant of H2-2-2 while were increased for the mutant of VHH_{hCG}. The change in the heat capacity (ΔC_P) of the mutant of H2-2-2 was 1.7 kJ/mol/K, which was one-third that of the mutant of VHH_{hCG}. The C54-C78 introduction led to the slight increase in ΔC_P of both mutants of H2-2-2 and VHH_{hCG} compared to their wild types.

With the obtained thermodynamic parameters and T_m, ΔG values at each temperature ($\Delta G(T)$s) were illustrated in Figure 22.

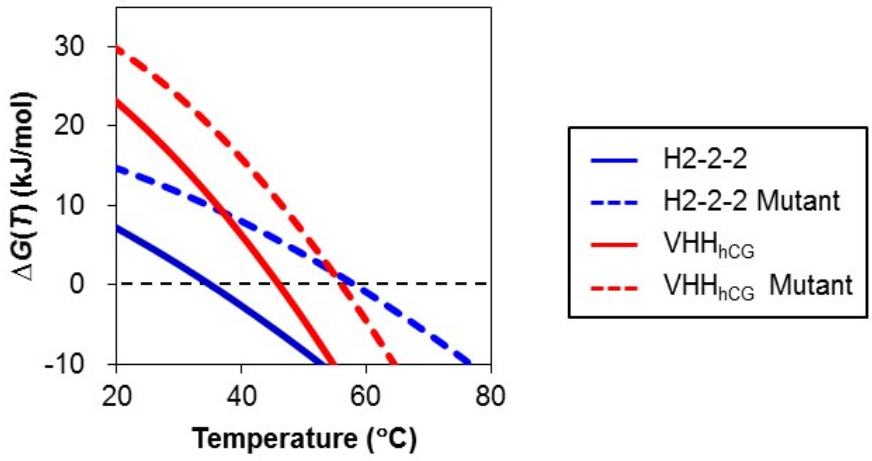

Figure 22. The free energy change of H2-2-2 (blue) and VHH_{hCG} (red). Solid lines indicate those of wild types and dashed lines indicate those of C54-C78 mutant.

Comparing the shape of $\Delta G(T)$ curves of mutants and wild types, C54-C78 introduction was seemed not to have large impact on $\Delta G(T)$ curve. The introduction of C54-C78 increased ΔG of H2-2-2 mutant and VHH_{hGC} mutant at T_m of wild type (T_m^W) to the same extent.

Figure 23 shows the differences in the change of free energy, enthalpy, and entropic term ($\Delta\Delta G$, $\Delta\Delta H$, and $-T\Delta\Delta S$) between H2-2-2 mutant and wild type at 35.1°C, which was the T_m value of the WT.

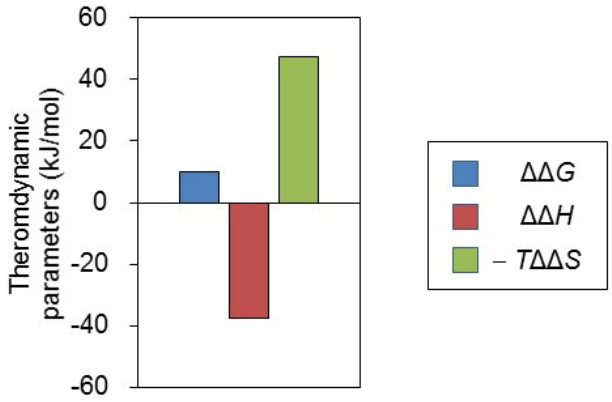

Figure 23. The differences in the thermodynamic parameter change between H-2-2-2 and its C54-C78 mutant at 35°C. The differences in the change of free energy ($\Delta\Delta G$), enthalpy ($\Delta\Delta H$) and entropic term ($-T\Delta\Delta S$) are indicated with the bars colored as in the figure.

It was found that $\Delta\Delta H$ was negative but largely compensated by $-T\Delta\Delta S$, resulting in a positive $\Delta\Delta G$.

To reveal the origin of larger T_m increase for H2-2-2 mutant than that of VHH_{hCG} mutant, thermodynamic parameters were examined. The ΔG increase at each T_m^W ($\Delta\Delta G(T_m^W)$) accompanied by the mutation was 9.9 kJ/mol for H2-2-2 and 10.4 kJ/mol for VHH_{hCG}, which were almost the same values as one another. Then, under the condition where $\Delta\Delta G(T_m^W)$ is a constant value, it was investigated that how the T_ms of mutant (T_m^W) changes when different values of other thermodynamic parameters are given. For simplification, at first, it considered the case where ΔC_P is zero and then ΔH and ΔS are constant. ΔG of mutant is indicated by Equation 5.

$$\Delta G = \Delta H - T\Delta S \quad (5)$$

Here ΔG at T_m^W is expressed as $\Delta G°$, while ΔG becomes zero at T_m^W, ΔH is indicated as Equations 6 and 7 from Equation 5.

$$\Delta H = \Delta G° + T_m^W \Delta S \quad (6)$$

$$\Delta H = T_m^M \Delta S \quad (7)$$

From Equations 6 and 7, T_m^M can be indicated as Equation 8.

$$T_m^M = T_m^W + \Delta G°/\Delta S \quad (8)$$

Thus,

$$\Delta T_m = T_m^M - T_m^W = \Delta G°/\Delta S \quad (9)$$

Equation 9 indicates that when ΔG^0 is unchanged, the smaller ΔS gives a larger ΔT_m. In fact, when the ΔS of the mutant of VHH_{hCG} (0.96 kJ/mol/K) was employed instead of that of the mutant of H2-2-2 (0.36 kJ/mol/K), the calculated ΔT_m of the mutant of H2-2-2 decreased from 27°C to 10°C. Next, the ΔG of the mutant of H2-2-2 was calculated when its ΔC_P (1.8 kJ/mol) takes zero or ΔC_P of the mutant of VHH_{hCG} (5.4 kJ/mol), under the condition that ΔG, ΔH and ΔS at T_m^W are unchanged (Figure 24).

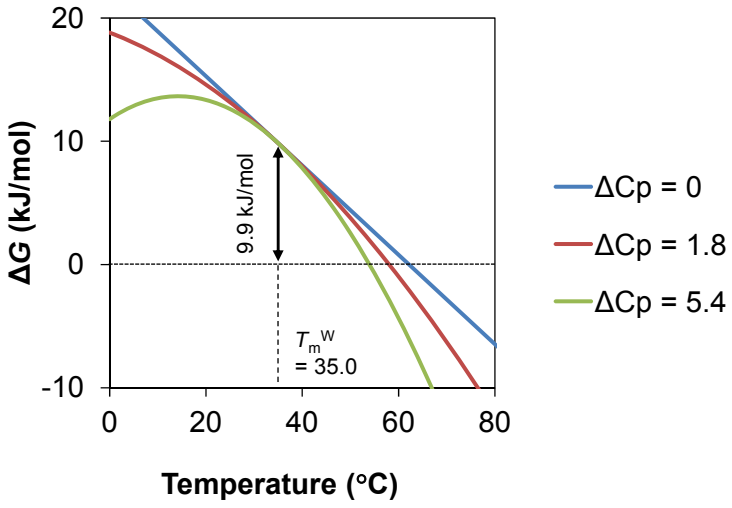

Figure 24. Simulation of $\Delta G(T)$ for H2-2-2 with different ΔC_P. The simulated $\Delta G(T)$ are indicated for H2-2-2 with ΔC_P values of 0 (blue line), 1.8 (red line) and 5.4 (green line) under the condition that ΔG, ΔH and ΔS at T_m^W are unchanged.

The smaller ΔC_P apparently resulted in the smaller ΔG temperature dependence, and ΔC_P of the mutant of H2-2-2 resulted in a ΔT_m of 23°C, which is higher than the ΔT_m (19°C) calculated using ΔC_P of the mutant of VHH_{hCG}. These estimations indicated that the small ΔS and ΔC_P values of the mutant of H2-2-2 could be causes of its higher ΔT_m.

As for the ΔG increase of the mutant of H2-2-2, Figure 23 suggested the contribution

of a large negative $\Delta\Delta S$. In order to have further thermodynamic insight into the effect of C54-C78 introduction to rVHs, experimental $\Delta\Delta S$ of H2-2-2 was compared with its theoretical entropy change of unfolded state by C54-C78 formation (ΔS_{calc}). In the classical chain-entropy model, an enhancement of stability by the S-S bond formation is primarily considered to be attributed to ΔS_{calc} (Flory PJ, 1956; Poland DG & Scheraga HA, 1965; Lin SH *et al.*, 1984; Pace CN *et al.*, 1988). The ΔS_{calc} can be calculated using an equation 10 (Poland DG & Scheraga HA, 1965).

$$\Delta S_{calc} = -R(3/2 \ln N + A) \quad (10)$$

where, R is the universal gas constant (8.31 J/mol/K) and N is the number of residues in the S-S bond-linked loops (21 residues). Constant A was proposed by Poland and Scheraga (Poland DG & Scheraga HA, 1965) and Pace *et al.* (Pace CN *et al.*, 1988) as 3.5 and 1.1, respectively. The ΔS_{calc} values were respectively calculated to −66.7 and −46.7 J/mol/K with each constant A. Both of the ΔS_{calc} values were far different from the experimentally obtained $\Delta\Delta S$ (−154.4 J/mol/K at 35.0°C), indicating that the classical chain-entropy model cannot be applied to rVH. Such a large discrepancy suggests that the restricted chain configuration of the unfolded state could not be the only effect of the C54-C78 introduction for H2-2-2. Changes in the internal interaction and/or hydration state might be other effects contributing to the mutant of H2-2-2 ΔG increase as reported for VHH_{hCG} (Hagihara Y *et al.*, 2007).

3.3. Summary of This Chapter

For industrial applications as therapeutic agents, a simple and universal method is strongly needed to enhance the thermal stability of rVHs. In this chapter, it was shown that introduction of additional S-S bond can highly thermally stabilize rVHs without severe loss of binding affinities. The unfolding temperature of rVHs stabilized by the S-S bond introduction were comparable to those of VHHs stabilized by the same method (Figure 20). It can be considered that this method for thermal stabilization is applicable not only to representative rVHs used in this section but also any other rVHs. Almost all (80–90%) of the rVHs have highly similar frameworks because of very limited germ-line gene segment (Borras L *et al.*, 2010; Kodangattil S *et al.*, 2014; Lavinder JJ *et al.*, 2014), and therefore the beneficial mutations in the framework could be shared among the rVHs.

Chapter 4

Improvement of Physical-Stabilities by Substitution with the Amino Acid Residues Conserved in VHHs

Many methods for improving the physicochemical properties of human VHs have been reported (To R *et al.*, 2005; Tanha J *et al.*, 2006; Barthelemy PA *et al.*, 2008; Perchiacca JM, 2012). One of the major ones is the substitution of amino acid residues with those conserved in camelid VHHs. For example, Davies *et al.* reported that a VH generated from human scFv, Ox13-VH, having a short transverse proton relaxation time in NMR spectroscopy, probably caused by aggregation through the exposed hydrophobic VL interaction surface, showed a normal value after the substitution of three residues located on the surface to mimic VHHs (Davies J & Riechmann L, 1994). In their other study, substitution of another two amino acids together with the introduction of an intradomain disulfide bond, which is frequently observed in VHHs, resulted in improved thermal stability of human VH (Davies J & Riechmann L, 1994). Such reports on human VH suggest that the introduction of conserved amino acids in VHH could be an attractive approach to improve the physicochemical properties of rVHs that also lack partner VLs.

In this section, the author focused on the amino acid residues which are conserved at the putative VL interaction interface and different between rVHs and VHHs. After identification of such amino acids and structural confirmation for their possibility to improve physico-chemical properties, amino acids in rVHs were strategically substituted with those in VHHs. First, it investigated the impacts of individual substitutions regarding the purification yield, antigen-binding affinity, thermal stability, and hydrophobicity of the molecular surface. Then, to improve the physicochemical properties further, multiple amino acid substitutions were introduced into rVHs. The findings in this section reveal that this approach is a rational and effective for improving the physicochemical properties of rVHs.

4.3. Materials and Methods

4.1.1. Comparison of Putative VL-Interaction Interface of rVHs with Corresponding Region of VHHs

To select the amino acid residues of rVHs for substitution with those of VHHs, the

author compared the amino acid residues of rVHs to VHHs, focusing on their region corresponding to the rVH-rVL interaction interface of rabbit Fv. In this study, all of the residues are numbered according to Kabat numbering (Kabat EA *et al.*, 1991) and "the residues of rVH located on rVL-interaction interface" were determined as the residues of rVHs within 5 Å from all residues of rVLs in the available PDB structures of rabbit Fv (PDB IDs: 4HBC, 4HT1, 4JO1, 4JO4, and 4O4Y) using Discovery Studio Ver 4.0. Amino acid sequences of rVHs obtained in this thesis and VHHs reported elsewhere (PDB IDs: 1HCV, 1BZQ, 1KXQ, 1OPQ, 1QD0, 1ZMY, and 1MEL) were then aligned with those of rVHs in rabbit Fvs, and the residues corresponding to "located on rVL-interaction interface" were identified for our rVHs and reported VHHs. Identified residues of our rVHs were compared with those of VHHs to select the candidate residues for substitution.

To estimate the physicochemical change accompanying a substitution, structural properties of candidate residues in rVHs and of corresponding residues in VHHs were investigated. For structural characterization, the ASA was measured for each candidate residue in the model structures of rVHs or the corresponding residue in the PDB structures of VHHs using Discovery studio. In addition, as described below, $\%ASA_{total}^{F}$ was calculated as the index of exposure and $\%ASA_{pol}$ as the index of hydrophilicity at the molecular surface.

$\%ASA_{total}^{F}$ was calculated using the following equation 11:

$$\%ASA_{total}^{F} = ASA_{total}^{F} / ASA_{total}^{UF} \times 100 \qquad (11)$$

where ASA_{total}^{F} and ASA_{total}^{UF} represent the ASA of total component atoms of the residue of interest (ASA_{total}) in the folded and unfolded protein. ASA_{total}^{F} was obtained as the ASA_{total} of the residue of interest in the model structures of rVHs or the PDB structures of VHHs. ASA_{total}^{UF} was obtained as the ASA_{total} of the residue of interest maximally exposed to the solvent in the center of tripeptides, which was created with Discovery studio to mimic the unfolded state of protein. These tripeptides consisted of three consecutive residues in the amino acid sequence of rVH, having a candidate residue in the center and the defined rotation angle of peptide bond ($\varphi = -120°$, $\psi = 120°$). $\%ASA_{pol}$ was calculated using the following equation 12:

$$\%ASA_{pol} = ASA_{pol} / ASA_{total}^{F} \times 100 \qquad (12)$$

ASA_{pol} was obtained from the model structure of rVHs or the PDB structures of VHHs.

4.1.2. Substitution with Preserved Amino Acid in VHHs

Amino acid residues of rVHs in the region corresponding to the rVL interaction interface were substituted with those of VHHs by site-directed mutagenesis. Substituted mutants were prepared by the same methods as wild type rVHs using *E. coli*.

4.1.3. Evaluation of Non-Specific Binding

Non-specific binding of rVHs was evaluated by ELISA. Purified rVHs were added at concentrations of 25, 50, and 100 nM to a Nunc MaxiSorp flat-bottomed 96-well plate, pre-coated with BSA. After washing with PBS (pH 7.4) containing 0.05% Tween-20, non-specifically bound rVHs were detected with HRP-conjugated anti-FLAG M2 antibody.

4.1.4. Evaluation of the Hydrophobicity of Molecular Surface

To evaluate the hydrophobicity of the molecular surface, rVH was subjected to HIC by a method similar to that described previously (Heldt CL *et al.*, 2017). The experiments were performed at 22°C using an Agilent 1100 HPLC System (Agilent, Santa Clara, CA, USA) with the TSKgel Butyl-NPR column (particle diameter 2.5 μm, inner diameter 4.6 mm, length 10 cm; TOSOH, Tokyo, Japan). Buffer A was 20 mM phosphate buffer (pH 6.9) supplemented with 2 M ammonium sulfate and buffer B was 20 mM phosphate buffer (pH 6.9). rVH was diluted with buffer A from 0.4 to 0.1 mg/mL, injected at a volume of 20 μL, and eluted with a linear gradient of increasing buffer B from 50% to 100% in 15 min at a flow rate of 1.0 mL/min.

4.1.5. Evaluation of Colloidal Stability

The size distributions of rVHs were analyzed using SV-AUC. SV-AUC experiments were performed using a Proteomelab XL-I Analytical Ultracentrifuge (Beckman-Coulter, Fullerton, CA, USA). rVH samples of 0.1 and 1.0 mg/mL in PBS (pH 7.4) were measured. Runs were carried out at 60,000 rpm at a temperature of 20°C using aluminum double sector centerpieces and a four-hole An60 Ti analytical rotor equilibrated to 20°C. The sedimentation boundary was monitored with UV detection optics at 231 nm for 0.1 mg/ml and at 289 nm for 1.0 mg/ml. At least 150 scans were collected between 6.00 and 7.25 cm from the center of the rotation axis. All SV-AUC raw data were analyzed by the

continuous C(s) distribution model using the software program SEDFIT14.4 (Schuck P, 2000). The position of the meniscus and the frictional ratio (f/f0) were varied as fitted parameters. Additional parameters for the analysis, which included partial specific volumes (H2-2-2 WT: 0.71 cm^3/g, H2-2-2 mutant with V37F/G44E/L45R/F91Y substitution: 0.71 cm^3/g), buffer density (ρ = 1.00 g/cm^3), and viscosity (η = 1.02 centipoises), were calculated using the SEDNTERP program (University of New Hampshire, USA). A resolution of 500 increments between 0 and 30 S was entered, and maximum entropy regularization was used (p = 0.68).

4.4. Results and Discussion

4.2.1. Determination of Amino Acid Residues for Substitution

In this chapter, it determined amino acid residues for substitution to improve physical-stabilities of rVHs. After different amino acid residues between rVHs and VHHs were identified in the putative VL-interacting interface, the possibilities were estimated for improvement of physico-chemical properties of rVHs by substitution with amino acid residues in VHHs, from the point of solvent exposure and surface hydrophilicity.

The different amino acid residues between rVHs and VHHs, which are conserved at the putative VL-interaction interface, were identified. The amino acid residues located at the putative VL-interaction interface of rVH model structures and PDB structures of VHH (PDB ID: 1HCV, 1BZQ, 1KXQ, 1OP9, 1QD0, 1ZMY, 1MEL) were shown in Figure 25.

		FR2							CDR2	FR3	FR4	
		37	39	43	44	45	46	47	57	91	103	105
rVH	H2-1-1	V	Q	K	G	L	E	W	F	F	W	Q
	H2-2-2	V	Q	K	G	L	E	W	A	F	W	Q
	H2-8	V	Q	E	G	L	E	W	W	F	W	Q
	H3-9	V	Q	K	G	L	E	W	Y	F	W	P
	H3-15	V	Q	K	G	L	E	Y	Y	F	W	Q
	H3-10	V	Q	K	G	L	E	W	Y	F	W	Q
	H3-12	V	Q	K	G	L	E	W	Y	F	W	P
	H3-13	V	Q	K	G	L	E	W	Y	F	W	P
	H3-14	V	Q	K	G	L	E	Y	W	F	W	Q
	H3-16	V	Q	K	G	L	E	W	W	F	W	Q
	H3-22	V	Q	K	G	L	E	W	W	F	W	Q
VHH	1HCV	F	Q	K	E	R	E	S	Y	T	W	Q
	1BZQ	F	Q	K	E	R	E	G	L	Y	W	Q
	1KXQ	F	Q	K	E	R	E	G	Y	Y	W	Q
	1OP9	F	Q	K	E	R	E	G	Y	Y	W	Q
	1QD0	F	Q	K	E	R	E	F	W	Y	W	Q
	1ZMY	F	Q	G	E	R	E	A	Y	Y	W	Q
	1MEL	F	Q	K	E	R	E	G	Y	Y	W	Q

Figure 25. Comparison of amino acid residues at the putative VL-interacting interface of rVHs and VHHs. Residues are numbered according to Kabat numbering (Kabat EA *et al.*, 1991). Amino acid residues, which are conserved in rVHs or VHHs, are indicated in white bold characters. Among them, ones that differ between rVHs and VHHs are surrounded by bold lines with blue (rVH) or red (VHH) background.

All of the amino acids except the 57th residue were conserved within most rVHs or within most VHHs, respectively. It was found that the 37th, 44th, 45th, 47th, and 91st residues differed between rVHs (Val, Gly, Leu, Trp, and Phe) and VHHs (Phe, Glu, Arg, Gly, and Tyr) among the conserved residues.

The 37th, 44th, 45th, 47th, and 91st residues of rVHs and VHHs were structurally compared from the point of solvent exposure. The extent of solvent exposure for each residue were estimated by calculating $\%ASA_{total}^{F}$, the index of exposure calculated according to the Materials and Methods. The $\%ASA_{total}^{F}$ of 37th, 44th, 45th, 47th, and 91st residues of rVHs and VHHs are indicated in Figure 26.

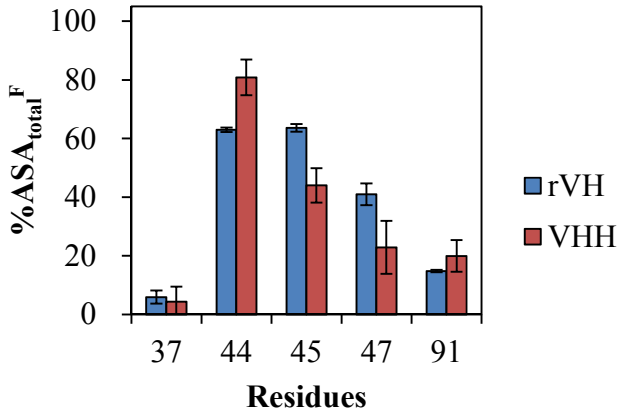

Figure 26. Calculated average values of $\%ASA_{total}^{F}$ for 37th, 44th, 45th, 47th, and 91st residues of rVHs and VHHs. Error bars indicate standard deviation among rVHs or VHHs.

The results showed that the residues in each position had similar $\%ASA_{total}^{F}$ values for rVHs and VHHs. The $\%ASA_{total}^{F}$ values were only 5.9% and 4.3% for V37 of rVHs and F37 of VHHs, respectively, indicating that the 37th residue is buried deep inside the structure. Meanwhile, because the $\%ASA_{total}^{F}$ values of the 44th and 45th residues were large (40%–80%) and those of the 47th and 91st residues were moderate (20%–40%), these residues were considered to be exposed largely or to some extent, respectively.

As for the 37th residue of rVHs, Val (V37) was found to be highly conserved (Figure 25) and estimated to be buried deep inside structure (Figure 26). In addition, V37 was surrounded by many hydrophobic amino acid residues (L45, W47, F91, F100i, and W103) in the model structure of rVHs (Figure 27).

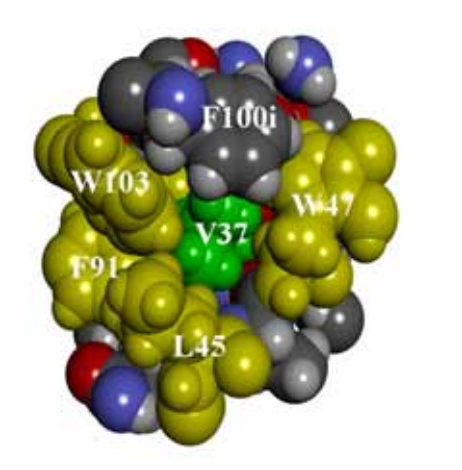

Figure 27. Amino acid residues around the V37 in H2-2-2 model structure. Residues are numbered according to Kabat numbering (Kabat EA *et al.*, 1991). Using Discovery studio, V37 (green) and residues around V37 (within 7 Å) in H2-2-2 model structure are indicated by CPK model. Residues substituted in this study with amino acids conserved in VHHs are shown in yellow.

While, Phe is conserved at the 37th residue of VHHs (Figure 25). It was expected that the substitution of V37, which is surrounded by hydrophobic residues, with bulky Phe would enhance packing in the internal hydrophobic core.

The 37th, 44th, 45th, 47th, and 91st residues of rVHs and VHHs were also structurally compared from the point of hydrophilicity. The contributions of hydrophilicity to molecular surface were estimated with $\%ASA_{pol}$, the index of hydrophilicity according to the Materials and Methods. At first, the $\%ASA_{pol}$ values were calculated for residues located in putative VL-interacting interface ($\%ASA_{pol}^{VH\text{-}VL}$), and compared with those for residues in other regions ($\%ASA_{pol}^{Others}$) (Figure 28).

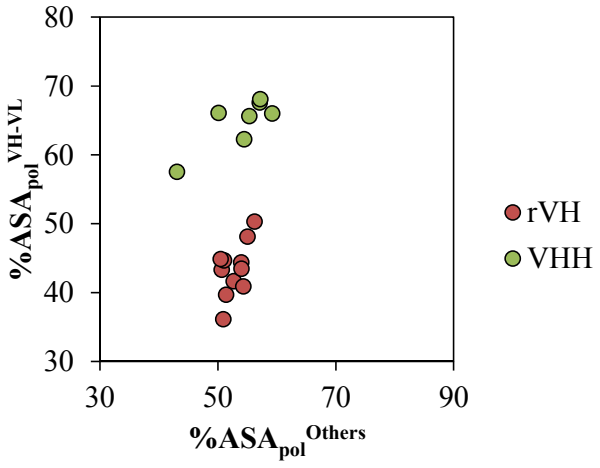

Figure 28. Comparison of $\%ASA_{pol}$ between rVHs and VHHs by regions. The $\%ASA_{pol}^{Others}$ (abscissa) and $\%ASA_{pol}^{VH-VL}$ (ordinate) of rVHs and VHHs are indicated as red circles and green circles, respectively.

It could be confirmed that a large difference in hydrophilicity is likely to exist mainly at the putative VL-interacting interface from the results that rVHs clearly had lower $\%ASA_{pol}^{VH-VL}$ values than VHHs while rVHs and VHHs showed similar $\%ASA_{pol}^{Others}$ values.

It then investigated $\%ASA_{pol}$s for each amino acid residues located on the putative VL-interacting interface. The $\%ASA_{pol}$s of 37th, 44th, 45th, 47th, and 91st residues of rVHs and VHHs were indicated in Figure 29.

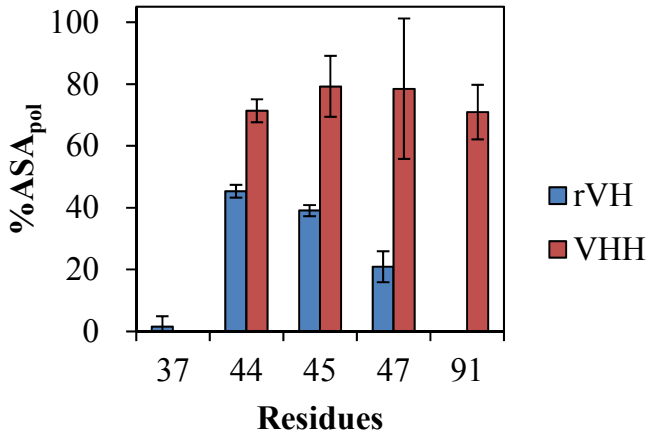

Figure 29. Calculated average values of $\%ASA_{pol}$ for 37th, 44th, 45th, 47th, and 91st residues of rVHs and VHHs. Error bars indicate standard deviation among rVHs or VHHs.

Among the five amino acid residues different between rVHs and VHHs in the putative VL-interacting interface, the 44th, 45th, 47th, and 91st amino acid residues in VHHs showed larger $\%ASA_{pol}$ values than those in rVHs. $\%ASA_{pol}$ values were also investigated for 39th, 43rd, 46th, 103rd, and 105th amino acid residues, in which the identical amino acids are adopted in rVHs and VHHs (Figure 30).

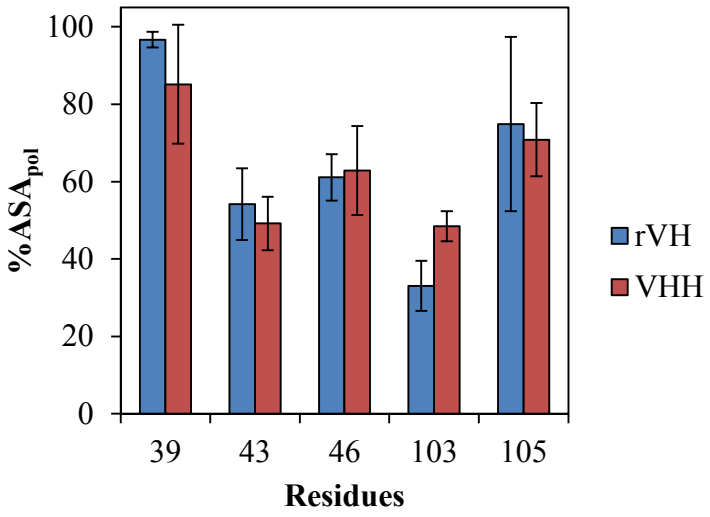

Figure 30. Comparison of $\%ASA_{pol}$ between rVHs and VHHs by residues. The average value of $\%ASA_{pol}$ was indicated for each residue of rVHs and VHHs as white and grey bars, respectively.

As a result, no differences were observed between the rVHs and VHHs in the $\%ASA_{pol}$ values of these amino acid residues. These findings indicate that the greater hydrophilicity of VL-interacting interface of VHHs is attributable to 44th, 45th, 47th, and 91st residues. It was therefore expected that substitutions of these four amino acid residues to those of VHHs increase the hydrophilicity at molecular surface of rVHs. Finally, side chain of 44th residue generated by substitution of Gly to Glu was confirmed to be exposed to the solvent in the model structures of the G44E mutants of rVHs constructed in Discovery studio.

4.2.2. Single Substitution Studies

HER2-specific H2-2-2 has high antigen-binding affinity, however, the expression level in *E. coli* is very low due to low conformational stability (Figure 14). Thus substitution studies were conducted using H2-2-2 as a model case.

H2-2-2 mutants with substitutions with amino acids conserved in VHH (V37F, G44E, L45R, W47G, and F91Y) were prepared using an *E. coli* expression system. After that, the

effects of these substitutions on purification yield, binding affinity, conformational stability, and molecular surface hydrophobicity were investigated. For the 44th and 45th residues, G44E/L45R double mutants were prepared by substituting the adjacent hydrophobic amino acids with hydrophilic ones. The purity of finally purified H2-2-2 mutants with substitutions was confirmed by the SDS-PAGE analysis (Figure 31).

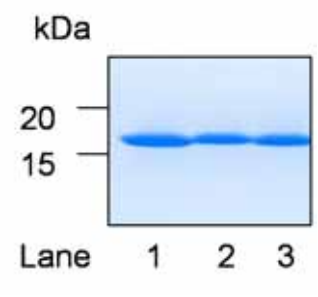

Figure 31. Confirmation of the purities of H2-2-2 mutants. About 2 μg of each purified proteins were loaded. Lane 1-3 correspond to H2-2-2 mutants (V37F, G44E/L45R, and F91Y, respectively).

As for W47G mutant, a sufficient amount of sample for biophysical characterization was not obtained due to a reduced expression level in soluble form (Figure 32).

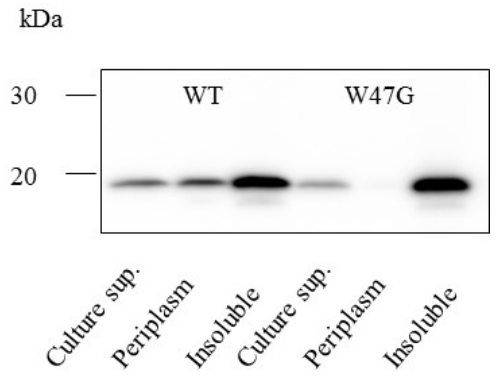

Figure 32. Comparison of the *E. coli* expression levels of H2-2-2 WT and mutant with W47 substitution. Western blotting of culture supernatant, periplasm and insoluble precipitate of *E. coli* expressing H2-2-2 WT or W47G mutant. For all fractions, the amount equivalent to 5 uL of culture solution was loaded and detected with HRP conjugated anti-FLAG M2 antibody (Sigma-Aldrich).

Table 14 shows the purification yield (purified amount of rVH obtained per liter of the culture), binding affinity to HER2 (K_D values in SPR analysis), thermal stability (T_{peak}

values in DSC analysis), and elution time in HIC of the mutants. Elution time in HIC was investigated as an index of hydrophilicity at the molecular surface.

Table 14. Properties of H2-2-2 mutants substituted with amino acids conserved in VHHs

	*Residues					Yield	T_{peak}	K_D	E. T.
	37	44	45	47	91	(mg)	(°C)	(nM)	(min)
WT	V	G	L	W	F	0.08	37.7	0.6	9.2
V37F	***F***	G	L	W	F	1.0	46.8	1.6	10.1
G44E/L45R	V	***E***	***R***	W	F	0.7	38.7	0.4	5.2
F91Y	V	G	L	W	***Y***	0.3	40.1	0.3	11.6

*The residues replaced by the VHH conserved amino acids are shown in bold-italic letters.

Yield: Purification yield obtained per liter of culture in the *E. coli* expression system.

T_{peak}: Temperature at which C_P peaks in the DSC analysis.

K_D: Dissociation constant for HER2 binding determined by SPR analysis.

E. T.: Elution time in HIC.

The purification yield of the V37F mutant was more than 10 times that of the H2-2-2 WT. The binding affinity of this mutant to HER2 was slightly decreased (the K_D value was 2.7 times greater than that of WT). As expected, the T_{peak} value was increased by nearly 10°C. This mutant was eluted somewhat later than the WT (delay of 0.9 min) in HIC, suggesting a slight increase in the hydrophobicity of the molecular surface. The purification yield of the G44E/L45R double mutant was 8.7 times higher than that of the WT. The HER2 binding affinity of the double mutant was almost equivalent to that of the WT, and the T_{peak} value was 1.0°C higher than that of the WT. The most prominent change shown by the substitutions was a markedly shorter HIC elution time (shortened by 4 min) than that of the WT, suggesting that the hydrophobicity of the molecular surface was greatly reduced. The purification yield of the F91Y mutant was 3.8 times higher than that of the WT. The binding affinity of the F91Y mutant was slightly higher than that of the WT (the K_D value was half that of the WT) and the T_{peak} value was increased by 2.4°C. F91Y mutant was eluted later than the WT in HIC (delay of 2.4 min), indicating that this mutation slightly increased the hydrophobicity of the molecular surface.

4.2.3. Thermodynamic Analysis of V37F Mutant

rVHs were thermally stabilized by focusing on V37, which is almost completely buried inside the structure (Figure 26), and its highly hydrophobic surroundings (Figure 27). To elucidate the thermodynamic origin of this marked enhancement in thermal stability by the V37F substitution, thermodynamic analysis of the H2-2-2 mutant with the V37F substitution was carried out by DSC (Figure 33).

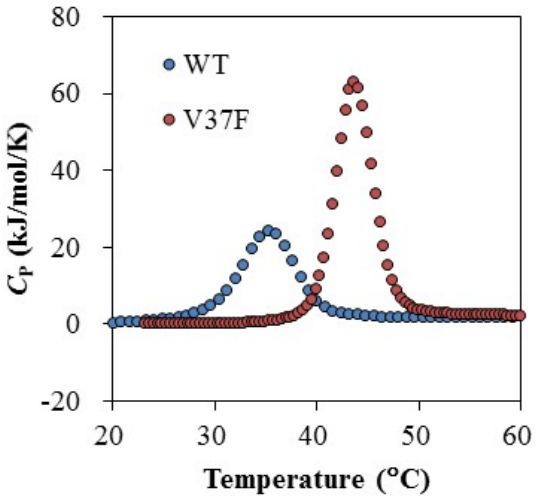

Figure 33. Thermodynamic analysis of rVH mutant with V37F substitution. The C_P curves of the WT and mutant with V37F substitution are presented by open and closed circles, respectively.

Thermodynamic parameters of the H2-2-2 WT and V37F mutant were obtained from DSC curve (Table 15).

Table 15. Thermodynamic parameters of H2-2-2 WT and V37F mutant

	T_m (°C)	ΔH (kJ/mol)	ΔS (kJ/mol/K)	ΔC_P (kJ/mol/K)
WT	35.1	161.4 ± 1.9	532.8 ± 6.0	1.5 ± 0.1
V37F	43.6	304.6 ± 11.7	961.6 ± 36.9	2.3 ± 0.2

The T_m value of the V37F mutant was 43.6°C, which was almost 10°C higher than that of the WT (35.1°C), consistent with the difference in T_{peak} values. In addition, the ΔC_P value of the V37F mutant was increased to 2.3 kJ/mol/K from 1.5 kJ/mol/K in the WT.

Based on the thermodynamic parameters shown in Table 15, the temperature dependences of the ΔG values were plotted (Figure 34).

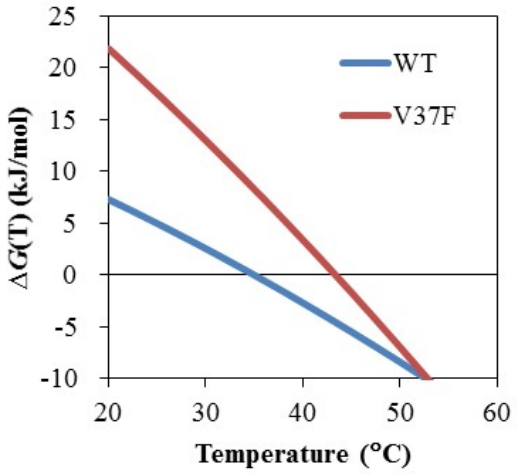

Figure 34. The Δ*G* curves of the WT and mutant with V37F substitution are presented by blue and red lines, respectively.

This showed that the maximum Δ*G* value of the V37F mutant was clearly greater than that of the WT. Figure 35 shows the differences in the changes of free energy, enthalpy and entropic term (ΔΔ*G*, ΔΔ*H*, and − *T*ΔΔ*S*) between the V37F mutant and the WT at 35.1°C, which was the T_m value of the WT.

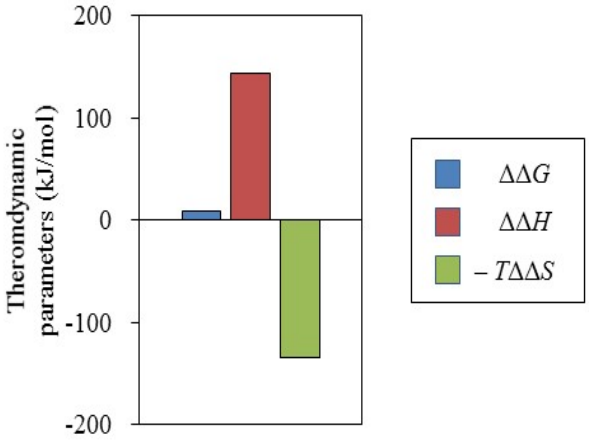

Figure 35. The differences in the thermodynamic parameters (ΔΔ*G*, ΔΔ*H*, − *T*ΔΔ*S*) between the WT and mutant with V37F substitution are presented by bars.

− *T*ΔΔ*S* showed a large negative value, however, ΔΔ*G* became positive as a result of the large positive ΔΔ*H* value. Namely, the mutant with the V37F substitution would be highly

thermally stabilized via increased free energy due to the enthalpic contribution, which exceeded the loss in the free energy owing to entropic change.

It was expected that hydrophobic packing inside the structure would be strengthened by replacing V37 of this hydrophobic core with Phe, which has a bulkier side chain. The importance of packing of hydrophobic cores for conformational-stability has been demonstrated for barnase (Kellis JT *et al.*, 1989), chymotrypsin inhibitor (Jackson SE *et al.*, 1993), human lysozyme (Takano K *et al.*, 1995), ribonuclease HII from hyperthermophile (Dong H *et al.*, 2008), cytochrome C (Liggins JR *et al.*, 1999), and others. When we introduced the V37F substitution, a great improvement of the thermal stability of H2-2-2 was shown (Table 14 and 15). From the thermodynamic analysis of H2-2-2, it was considered that the mutant with the V37F substitution was highly thermally stabilized via increased free energy due to the enthalpic contribution, which exceeded the loss in the free energy owing to entropic change (Figure 35). These changes in thermodynamic parameters suggest two phenomena indicating a tightening of the packing structure: a decrease in the flexibility of the native state structure and an increase in the interaction inside this structure. In the case of human lysozyme, when a mutation intended to attenuate hydrophobic packing was introduced, the thermodynamic parameter changed in the opposite direction to that in this study, leading to thermal destabilization (Takano K *et al.*, 1995). This also supports the concept that the V37F substitution enhanced the thermal stability of H2-2-2 through tightening the hydrophobic packing.

4.2.4. Combination Substitution Studies

To examine the effect of combined substitutions on H2-2-2, a triple mutant was produced by introducing the V37F substitution, which greatly improved thermal stability, and the G44E/L45R substitutions, which greatly reduced the hydrophobicity of the molecular surface. After that, F91Y substitution, which slightly enhanced thermal stability in single substitution study, was additionally introduced. V37F/G44E/L45R triple mutant and V37F/G44E/L45R/F91Y quadruple mutant of H2-2-2 were prepared and the purity of their purification sample was confirmed by SDS-PAGE analysis (Figure 36).

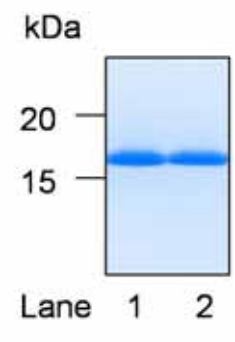

Figure 36. Confirmation of the purities of V37F/G44E/L45R (Lane1) and V37F/G44E/L45R/F91Y mutant (Lane 2). About 2 μg of each purified proteins were loaded.

Using purification sample, properties of V37F/G44E/L45R and V37F/G44E/L45R/F91Y mutant were investigated and summarized in Table 16.

Table 16. Properties of V37F/G44E/L45R and V37F/G44E/L45R/F91Y mutant of H2-2-2

	*Residues					Yield	T_{peak}	K_D	E. T.
	37	44	45	47	91	(mg)	(°C)	(nM)	(min)
V37F/G44E/L45R	***F***	***E***	***R***	W	F	3.3	47.9	1.6	4.6
V37F/G44E/L45R/F91Y	***F***	***E***	***R***	W	***F***	3.5	49.4	1.2	4.6

*The residues replaced by the VHH conserved amino acids are shown in bold-italic letters.

Yield: Purification yield obtained per liter of culture in the *E. coli* expression system.

T_{peak}: Temperature at which C_P peaks in the DSC analysis.

K_D: Dissociation constant for HER2 binding determined by SPR analysis.

E. T.: Elution time in HIC.

Surprisingly, the purification yield of V37F/G44E/L45R mutant was more than 40 times that of the WT (3.3 mg per liter of medium). In addition, the K_D of this mutant was 1.6 nM, equivalent to that of the mutant with the single substitution of V37F. The T_{peak} value was 47.9°C and the effect of the triple substitutions on this variable regarding thermal stabilization was almost consistent with the sum of the effects of single and double substitutions (T_{peak} increases of 9.1°C and 1.0°C, respectively). Furthermore, the elution time in HIC was shortened to 4.6 min from 5.2 min for the G44E/L45R mutant, suggesting that the addition of the V37F mutation further reduced the hydrophobicity. Regarding to

V37F/G44E/L45R/F91Y mutant, the purification yield was not affected by the additional substitution of F91Y (3.5 mg per liter of medium). The HER2 binding affinity was also almost equivalent to that of the parental V37F/G44E/L45R mutant (K_D = 1.2 nM). Since the elution time in HIC was the same as that of the parental mutant (4.6 min), it was considered that the hydrophobicity of the molecular surface was unchanged. While, T_{peak} value of this mutant was 49.4°C, which was 1.5°C higher than that of parental mutant.

When the W47G substitution was added to the V37F/G44E/L45R triple mutant, the expression level in soluble form dramatically decreased. This meant that a sufficient amount for evaluations could not be obtained for this quadruple mutant, similar to the case for the W47G single mutant with substitution.

4.2.5. Further Investigation of V37F/G44E/L45R/F91Y Mutant

With regard to the V37F/G44E/L45R/F91Y quadruple mutant of H2-2-2, which showed improved physicochemical properties such as reduced hydrophobicity, its non-specific binding was evaluated by ELISA against BSA (Figure 37).

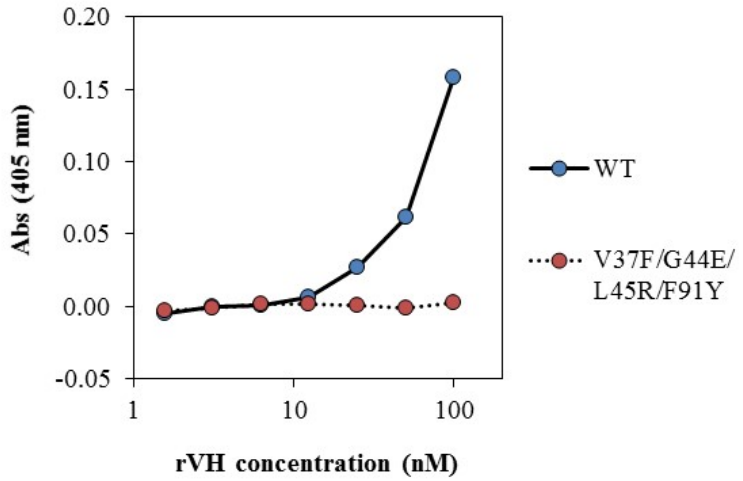

Figure 37. Evaluation of non-specific binding of the quadruple mutant by ELISA. Non-specific binding was indicated as an assay signal (absorbance at 405 nm) of ELISA toward a BSA-coated plate. The indicated values are assay signals from which the blank signals had been subtracted.

While H2-2-2 WT showed concentration-dependent non-specific binding to BSA-coated plates, this mutant exhibited no binding even at the maximum concentration of 100 nM.

Next, to compare colloidal stability, the size distributions of rVHs were evaluated by SV-AUC. At the solution concentrations measured (0.1 or 1.0 mg/mL), rVHs are

considered to undergo ideal sedimentation. The results indicated the concentration-dependent self-association of H2-2-2 WT (Figure 38).

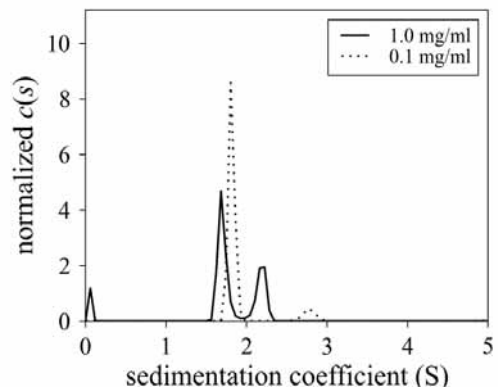

Figure 38. Distribution of normalized C(s) sedimentation coefficient obtained from SV-AUC experiments. Those for H2-2-2 WT at 0.1 mg/mL (dashed line) and 1.0 mg/mL (solid line).

H2-2-2 WT with a sedimentation coefficient of more than 2 S is a self-associated species, for which the amount increased at 1.0 mg/mL compared with that at 0.1 mg/mL. On the other hand, no self-associated fraction was observed for the quadruple mutant of H2-2-2 with V37F/G44E/L45R/F91Y substitutions, even at 1.0 mg/mL, indicating that these quadruple substitutions enhanced the colloidal stability of H2-2-2 (Figure 39).

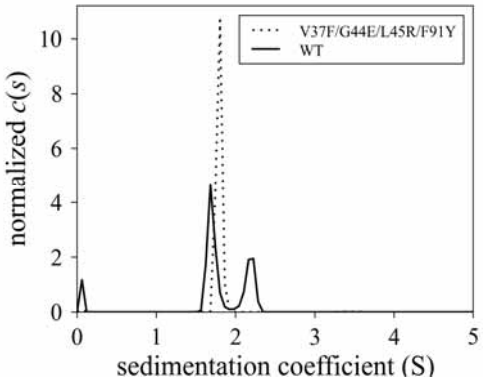

Figure 39. Distribution of normalized C(s) sedimentation coefficient obtained from SV-AUC experiments. Those for H2-2-2 WT (solid line) and its mutant with V37F/G44E/L45R/F91Y substitutions (dashed line) at 1.0 mg/mL.

4.2.6. Consideration for Change in the Hydrophilicity of Molecular Surface

Amino acid residues in rVHs were substituted with those of VHHs to enhance the hydrophilicity at the molecular surface in the previous sections. Because there was a difference in $\%ASA_{pol}$ values between rVHs and VHHs only at the putative VL-interacting interface (Figure 29), the residues at this interface were selected for substitution. Among the residues in the region corresponding to the this interface of rVHs, the 44th, 45th, 47th, and 91st residues showed apparently lower $\%ASA_{pol}$ than those of VHHs (Figures 29 and 30). Upon substituting these residues with those of VHHs, the elution time of H2-2-2 in HIC showed various changes (Tables 14 and 16). To investigate the relations between structurally calculated values and experimentally obtained data, the elution times of H2-2-2 and its mutants in HIC was plotted to the $\%ASA_{pol}^{VH-VL}$ values calculated from their model structures, which were constructed with Discovery studio (Figure 40).

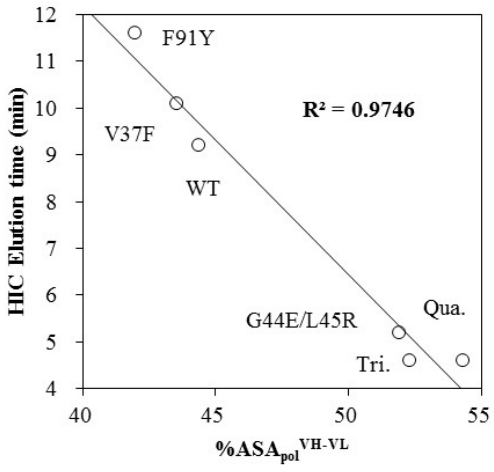

Figure 40. The inverse correlation between elution time in HIC and $\%ASA_{pol}^{VH-VL}$. For H2-2-2 WT and its mutants, elution times in HIC and $\%ASA_{pol}^{VH-VL}$ are plotted. Tri. and Qua. indicates the triple mutant with V37F/G44E/L45R substitutions and the quadruple mutant with V37F/G44E/L45R/F91Y substitutions. The square of the correlation coefficient (R^2) is shown in bold.

It was interestingly found that the elution times in HIC inversely correlated well with the $\%ASA_{pol}^{VH-VL}$ values ($R^2 = 0.98$).

Subsequently, the changes in ASA_{pol} (ΔASA_{pol}) and $ASA_{non-pol}$ ($\Delta ASA_{non-pol}$) of each residue accompanying the substitutions from the WT to mutants were calculated. The calculated ΔASA_{pol} and $\Delta ASA_{non-pol}$ of each residue in V37F, G44E/L45R, F91Y single

or double mutant, V37F/G44E/L45R triple and V37F/G44E/L45R/F91Y quadruple mutant were indicated in Table 17.

Table 17. ΔASA_{pol} and $\Delta ASA_{non\text{-}pol}$ of each residue from H2-2-2 WT to each mutant with substitutions

	Residue	37	39	43	44	45	46	47	57	91	103	105	Total
	Amino acid	V	Q	K	G	L	E	W	A	F	W	Q	
V37F	ΔASA_{pol}	0	**-15**	2	-2	-3	0	7	0	0	**10**	-9	**-10**
	$\Delta ASA_{non\text{-}pol}$	**16**	3	-2	2	**17**	-4	**37**	-1	**-20**	**-48**	4	4
G44E/L45R	ΔASA_{pol}	0	4	-2	**87**	3	0	2	2	0	6	8	**111**
	$\Delta ASA_{non\text{-}pol}$	-4	1	**17**	**15**	-7	0	**-14**	9	-3	**-34**	1	**-18**
F91Y	ΔASA_{pol}	0	**-21**	3	-2	**-11**	3	-4	2	**24**	1	-2	-8
	$\Delta ASA_{non\text{-}pol}$	4	2	-2	2	7	-5	**38**	7	**-20**	1	3	**37**
Triple	ΔASA_{pol}	0	2	3	**85**	**21**	2	**17**	0	0	-1	**-14**	**116**
	$\Delta ASA_{non\text{-}pol}$	5	0	-2	**16**	5	**-10**	**-21**	-5	-1	-9	3	**-20**
Quadruple	ΔASA_{pol}	0	-5	3	**94**	**27**	3	**15**	1	**29**	2	**-14**	**155**
	$\Delta ASA_{non\text{-}pol}$	**13**	0	-3	**15**	-3	-7	**-21**	6	**-17**	-9	3	**-22**

Triple: Triple mutant with V37F/G44E/L45R substitution.

Quadruple: Triple mutant with V37F/G44E/L45R/F91Y substitution.

$\%ASA_{pol}$: The change in ASA_{pol} from WT to each mutant with substitutions (Å)

$\%ASA_{non\text{-}pol}$: The change in $ASA_{non\text{-}pol}$ from WT to each mutant with substitutions (Å)

The numbers which indicate large positive effect to hydrophilicity ($\Delta ASA_{pol} > 10$ Å or $\Delta ASA_{non\text{-}pol} < -10$ Å) are colored in blue with bold letter.

The numbers which indicate large negative effect to hydrophilicity ($\Delta ASA_{pol} < -10$ Å or $\Delta ASA_{non\text{-}pol} > 10$ Å) are colored in red with bold letter.

Positive ΔASA_{pol} and negative $\Delta ASA_{non\text{-}pol}$ values were considered to contribute to the enhanced hydrophilicity. Using these data and calculated values, how each substitution affected the hydrophilicity is discussed.

At the 44th and 45th residues of rVHs, Gly and Leu were highly conserved (Figure 25) and well exposed to the solvent when lacking their corresponding rVLs (Figure 26). In contrast, Glu and Arg were conserved at these positions in VHHs (Figure 25) and largely exposed to the solvent as well (Figure 26). Since the proportion of exposed polar components in these residues was higher in VHHs than in rVHs (Figure 29), substitution to amino acids that are conserved in VHHs was expected to enhance the hydrophilicity of the molecular surface of rVHs. When the G44E/L45R substitution was introduced into

H2-2-2, the elution time in HIC became considerably shorter than that of the WT (Table 14), indicating less hydrophobicity of the molecular surface, as expected. According to Table 17, G44E substitution probably made a direct contribution to hydrophilic enhancement, through the ASA_{pol} increase and the $ASA_{non\text{-}pol}$ decrease at this residue itself. Meanwhile, L45R might have indirectly contributed to hydrophilicity. In the model structure of the H2-2-2 mutant with G44E/L45R substitutions, large positive changes in the ASA were observed not for L45R itself but for W47 and W103, which were spatially close to L45 (Figure 27).

Regarding the 91st residue, because the $\%ASA_{pol}$ value of Y91 in VHHs was rather higher than that of F91 in rVHs (Figure 29), F91Y substitution was considered to enhance the hydrophilicity of the molecular surface. It was therefore unexpected that F91Y substitution resulted in a prolonged elution time of H2-2-2 in HIC (Table 14). There is a possibility that F91Y substitution could have increased ASA_{pol} and decreased $ASA_{non\text{-}pol}$ of this residue itself, but resulted in a decrease of hydrophilicity due to influences on other residues (Table 17). However, when F91Y substitution was introduced into the triple mutant with V37F/G44E/L45R substitutions, the substitution could have a positive influence to hydrophilicity of this residue itself without having a negative influence to hydrophilicity on other residues (Table 17). Simultaneous substitutions of V37F, L45R, and F91Y may have caused reconstitution of the hydrophobic core around V37 of rVHs (Figure 27) to surroundings similar to those of VHHs, which can accept Tyr at the 91st residue.

4.2.7. Consideration for Folding of Mutants with Substitutions

It can be considered that rVHs are properly folded even after substitutions were introduced based on three experimental evidences below; (i) rVH mutants showed similar target binding activities as their WT in SPR analysis (Tables 14 and 16), and (ii) rVH mutants showed thermal unfolding profiles with obvious endothermic heats, T_{onset}s and T_ms as their WT in DSC analysis (Tables 14 and 16). (iii) Experimentally estimated value of sedimentation coefficient (*S* value) for H2-2-2 quadruple mutant was 1.78S (Figure 39), close to 1.71S which is the *S* value calculated from the three-dimensional coordination of the mutant modeled structure. Owing to the recent extensive researches, it has been recognized that *S* value of a protein that reflects hydrodynamic properties of the protein can be calculated based on the three-dimensional coordination of the protein using programs with a program SOMO (SOlution MOdeller) equipped with the UltraScan 3 software (Rocco M & Byron O, 2015).

4.2.8 Substitution studies for another rVH

The improvement of physicochemical properties associated with amino acid substitutions was also studied with H2-1-1, which is another HER2-specific rVH. First, triple mutations of V37F/G44E/L45R, which highly improved physical-stabilities of H2-2-2, were introduced. After that, F91Y substitution was additionally introduced into the triple mutant with V37F/G44E/L45R substitutions. The purity of purified V37F/G44E/L45R and V37F/G44E/L45R/F91Y mutants of H2-1-1 was confirmed by SDS-PAGE (Figure 41).

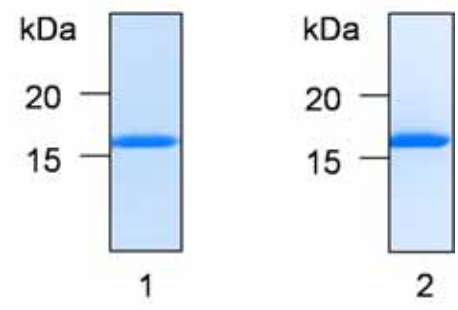

Figure 41. Confirmation of the purities of V37F/G44E/L45R (Lane 1) and V37F/G44E/L45R/F91Y (Lane 2) mutants of H2-1-1. About 2 μg of each purified proteins were loaded.

Using purification sample, properties of V37F/G44E/L45R and V37F/G44E/L45R/F91Y mutants were investigated and summarized in Table 18.

Table 18. Properties of H2-1-1 WT and its V37F/G44E/L45R and V37F/G44E/L45R/F91Y mutants

	*Residues					Yield	T_{peak}	K_D
	37	44	45	47	91	(mg)	(°C)	(nM)
WT	V	G	L	W	F	0.003	48.1	28
V37F/G44E/L45R	***F***	***E***	***R***	W	F	2.5	56.0	19
V37F/G44E/L45R/W47G	***F***	***E***	***R***	***G***	F	0.2	40.2	29
V37F/G44E/L45R/F91Y	***F***	***E***	***R***	W	***Y***	3.6	55.9	18

*The residues replaced by the VHH conserved amino acids are shown in bold-italic letters.

Yield: Purification yield obtained per liter of culture using *E. coli* expression system.

T_{peak}: Temperature at which C_P peaks in the DSC.

K_D: Dissociation constant for HER2 binding determined by SPR analysis.

In chapter 2, since the purification yield of H2-1-1 in an *E. coli* expression system was further lower than that of H2-2-2, it had to use mammalian cell expression system to prepare H2-1-1 WT. However, with V37F/G44E/L45R substitutions, the purification yield in the *E. coli* expression system was dramatically improved to more than 800 times higher than that with WT. The HER2 binding affinity of this mutant was equal to or higher than that of the WT (K_D = 19 nM), and its T_{peak} value was 56.0°C, which is almost 8.0°C higher than that of the WT. When F91Y mutation was additionally introduced to triple mutant, little influence was observed for purification yield, binding affinity, and thermal stability. On the other hand, additional W47G mutation to triple mutant exerted a marked negative effect on purification yield. Although this quadruple mutant with V37F/G44E/L45R/W47G substitutions retained the same degree of HER2 binding affinity as the WT, its T_{peak} value was lower than that of the parental triple mutant by almost 16°C.

4.2.9. Consideration for W47G mutation

The additional introduction of the W47G substitution also abolished the purification yields of H2-2-2 WT and V37F/G44E/L45R triple mutants of H2-1-1 and H2-2-2. Considering that the thermal stability of the H2-1-1 mutant with V37F/G44E/L45R substitutions was dramatically reduced by W47G substitution (Tables 18), the drastic reduction in purification yield was probably caused by structural destabilization. The

model structures of H2-2-2 WT showed that the aromatic ring of W47 interacts with the alkyl groups of A57 and A60 that were located at the region spatially close to W47, so as to bundle the long loop of CDR2 (Figure 42).

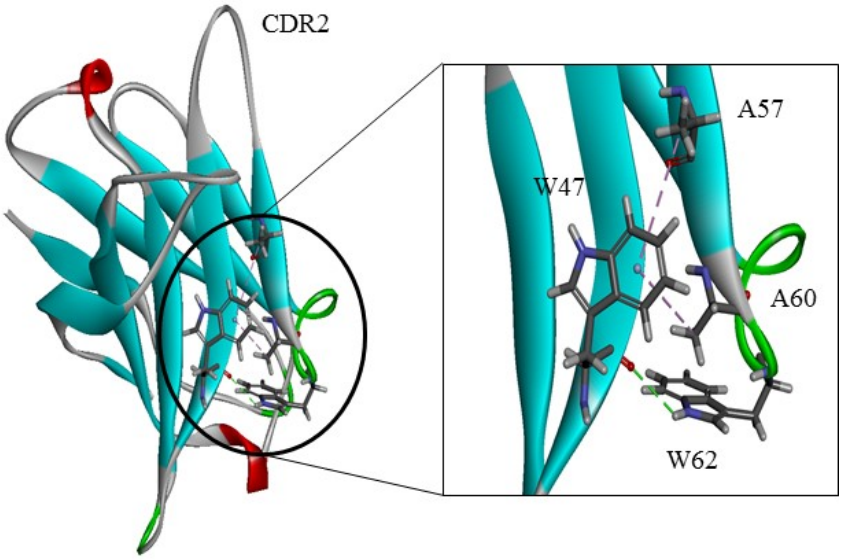

Figure 42. Interactions related to W47 in the modeled structure of H2-2-2 WT. Using Discovery studio, the interactions related to W47 in the modeled structure of H2-2-2 are displayed. The O atom of the W47 main chain was hydrogen bonded with the H atom of the W62 side chain. The side chain of W47 formed cation-π interaction with the side chains of A57 and A60. W47 is located at the N-terminus of CDR2 while A57, A60 and W62 are located at the opposite terminus.

Based on previous studies showing that cation-π interactions enhance the binding energy by 8–20 kJ/mol (Dougherty DA, 2013), deletion of the W47 side chain could result in the loss of tens of kJ/mol. From the Δ*G* curve shown in Figure 34, it can be understood that the parallel shift downwards of 10 kJ/mol, for example, results in a decrease of more than 10°C in the T_{peak} value. Such a substitution should be avoided, even if it can reduce the hydrophobicity of the molecular surface.

4.2.10. Consideration for Relation Between Conformational-Stability, Hydrophilicity, and Purification yield

In terms of the purification yield in the *E. coli* expression system, V37F substitution, which largely increased thermal stability, provided great improvement (Table 14). This would be in accordance with the correlation between the thermal stability and the purification yield as demonstrated in chapter 2. On the other hand, the purification yield

with G44E/L45R substitutions unexpectedly showed great improvement despite its low thermal stabilization effect (Table 14). In addition, the purification yield was improved by F91Y substitution to a lesser extent than G44E/L45R substitutions, even though F91Y substitution thermally stabilized H2-2-2 more than G44E/L45R substitutions (Table 14). Based on these findings, the author inferred that not only conformational stability but also hydrophilicity is an important factor for purification yield. During investigation of the relationships among the thermal stability, hydrophilicity, and purification yield of rVHs, significant correlations was found (Figure 43).

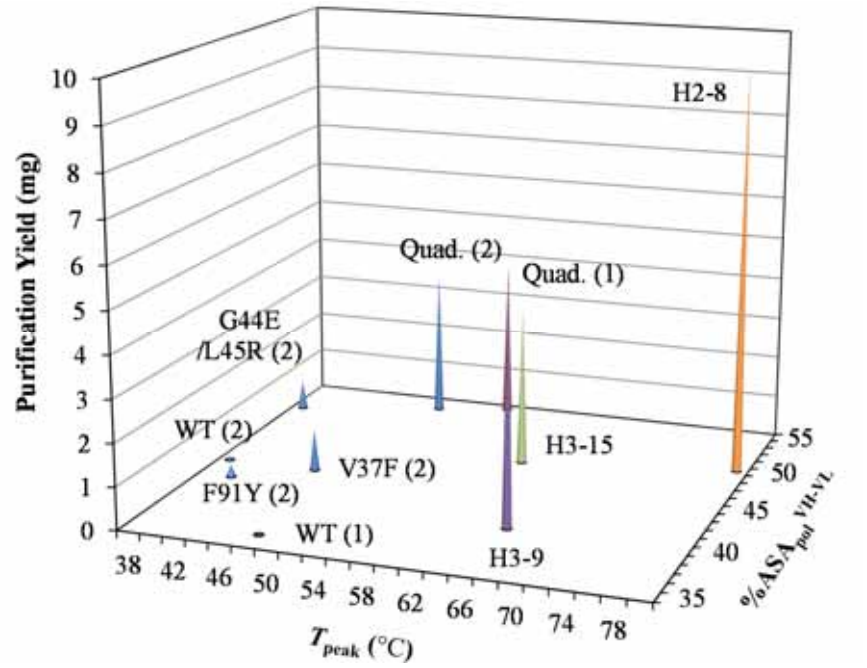

Figure 43. The relationships among thermal stabilities, hydrophilicities and purification yields of rVHs. For rVHs and their mutants, T_{peak} values (°C), %ASA_{pol}^{VH-VL} values and purification yields per 1L of culture medium (mg) are plotted. The T_{peak} values and purification yields of H2-8, H3-9 and H3-15 are quoted from the data in chapter 2. Quad. indicates the quadruple mutant with V37F/G44E/L45R/F91Y substitutions. The number "1" with parentheses indicates H2-1-1 and "2" indicates H2-2-2.

Quadruple mutants of H2-1-1 and H2-2-2, whose T_{peak} and ASA_{pol}^{VH-VL} values were both improved by V37F/G44E/L45R/F91Y substitutions, showed highly enhanced purification yields. In addition, all of H2-8, H3-9, and H3-15, whose purification yields were high (Figure 14), had high T_{peak} and ASA_{pol}^{VH-VL} values. These findings support our hypothesis that both conformational stability and hydrophilicity are important for high purification yields.

4.3. Summary of This Chapter

In this chapter, physico-chemical properties of two rVHs were improved without losing the binding affinity by substitutions with amino acid residues which are conserved in the putative VL-interacting interface of VHHs. Such an engineering for improvement was successfully achieved based on the comparison of three-dimensional structural properties between rVHs and VHHs. Through the studies, not only the method to improve physico-chemical properties of rVHs was constructed but also experimental information for designing physico-chemically beneficial mutations was obtained.

The author consider the mutant with V37F/G44E/L45R/F91Y substitutions as the most optimized one. Thermal stabilization of this mutant was achieved by enhancement of hydrophobic packing. Non-specific binding and colloidal stability were also greatly improved through reduction in the hydrophobicity of the molecular surface. Another phenomenon suggested improvements in physicochemical properties in this mutant. Specifically, when H2-2-2 WT at 1.0 mg/mL was frozen and thawed, aggregation leading to the formation of a white precipitate was observed. However, the optimized mutant did not precipitate at all after the freeze/thaw process. This phenomenon was considered to be due to the improvement of thermal and colloidal stabilities (Uchiyama S, 2014; Carpenter JF *et al.*, 2009).

Chapter 5

General Conclusions

The author demonstrated the possibility of obtaining rVHs with strong binding affinities (chapter 2), which have been difficult to be achieved by mouse or human-derived sdAbs, based on the hypothesis that a single variable region of IgG-type antibody with very high affinity could possess high affinity. Some obtained rVHs showed low conformational stabilities and purification yields. This fact implied that lowering temperature on phage production was the key to achieve efficient obtainment of rVHs. Obtained rVHs including those with concern of low physical-stabilities were subjected to two different type of protein-engineering modifications. Introduction of additional S-S bond largely enhanced conformational stabilities by entropic contribution (chapter 3). While substitution with amino acid residues conserved in VHHs improved conformational and colloidal stabilities of rVHs (chapter 4). Because both of approaches have not largely affected to binding affinities, these approach were considered to be useful for improving physical-stabilities of rVHs. Since rVHs are known to have almost common frameworks, such modifications are expected to be applicable to not only rVHs of this thesis but any other rVHs. The selectability of two different type of modifications for physical-stabilization may further expand the usability of rVHs.

Through this thesis, the possibility of rVH to be the source of sdAb with strong binding affinity and high availability was indicated. By utilizing rVHs, the further brisk of sdAb research and development, and eventually the creation of innovative pharmaceuticals contributing to the healthy and prosperous lives of people around the world could be expected.

List of Abbreviations

ADC	Antibody-Drug-Conjugate
AMD	Age-related Macular Degeneration
ASA	Accessible Surface Area
BSA	Bovine Serum Albumin
cDNA	complementary DNA
DSC	Differential Scanning Calorimetry
E. coli	*Escherichia coli*
ELISA	Enzyme Linked Immunosorbent Assay
Fab	Fragment antigen binding
Fc	Fragment crystalizable
FW	Framework
Hcab	Heavy chain-only antibody
FcRn	Neonatal Fc receptor
Fv	Fragment variable
HRP	Horseradish Peroxidase
hRSV	human Respiratory Syncytial Virus
HSA	Human Serum Albumin
HIC	Hydrophobic Interaction Chromatography
IL-6R	Interleukin-6 Receptor
mRNA	messenger RNA
MS	Mass Spectrometry
MW	Molecular Weight
PBS	Phosphate Buffered Saline
PCR	Polymerase Chain Reaction
PDB	Protein Data Bank
scFv	single-chain Fv
sdAb	single-domain Antibody
SDS-PAGE	Sodium Dodecyl Sulfate-Polyacrylamide Gel Electrophoresis
SEC-MALS	Size Exclusion Chromatography with Multi-Angle Light Scattering
SPR	Surface Plasmon Resonance
SV-AUC	Sedimentation Velocity Analytical Ultracentrifugation
RI	Radio-Isotope

RMSD	Root Mean Square Deviation
VH	Variable region of Heavy chain
VHH	Variable region of Heavy chain of Heavy chain antibody
VL	Variable region of Light chain
WB	Western Blotting
WT	Wild type

Acknowledgement

At first, I would like to really thank my graduate supervisor, Professor Susumu Uchiyama. Thank you for taking a lot of times to supervise, helpful discussions, suggestions, guidance, and encouragement during the course of my work. Also I would like to thank Professor Masahiro Kino-oka and Professor Takeshi Omasa for critical reading the thesis and giving sophisticated suggestions to my research.

I would very much appreciate providing me a great opportunity by Dr. Tohru Takahashi. I also have to thank Dr. Ryuji Hashimoto for fruitful discussions, providing great ideas, and encouragement. I thank our Daiichi Sankyo colleagues: Drs. Masakazu Tamura, Chikako Suzuki and Jun Hasegawa for critical reading of the manuscript and beneficial discussion and Drs. Masato Amano, Ryuki Miyauchi, Kensuke Nakamura, and Nobumi Nagaoka for supporting experiments. Mr. Masanori Noda also supported my experiments.

Finally, great thanks to my lovely family members, Taeko, Mikiya and Misaki for cooperation and cheering.

References

Abdin, S. M., Zaher, D. M., Arafa, E. A., Omar, H.A. Tackling cancer resistance by immunotherapy: Updated clinical impact and safety of PD-1/PD-L1 inhibitors. *Cancers (Basel)* **10,** doi: 10.3390/cancers10020032. (2018).

Alston, T. A. Morphine Zwitterion. *J Anesth Hist.* **3,** 69-70 (2017).

Arai, H., Glabe, C., Luecke, H. Crystal structure of a conformation-dependent rabbit IgG Fab specific for amyloid prefibrillar oligomers. *Biochim. Biophys. Acta.* **1820,** 1908–1914 (2012).

Arbabi-Ghahroudi, M. *et al.* Aggregation-resistant VHs selected by in vitro evolution tend to have disulfide-bonded loops and acidic isoelectric points. *Protein Eng. Des. Sel.* **22,** 59–66 (2009).

Bannas, P., Hambach, J., Koch-Nolte, F. Nanobodies and nanobody-based human heavy chain antibodies as antitumor therapeutics. *Front Immunol.* **8,** doi: 10.3389/fimmu.2017.01603. (2017).

Barthelemy, P. A.*et al.* Comprehensive analysis of the factors contributing to the stability and solubility of autonomous human VH domains. *J. Biol. Chem.* **283,** 3639–3654 (2008).

Behdani, M. *et al.* Development of VEGFR2-specific nanobody *Pseudomonas* exotoxin A conjugated to provide efficient inhibition of tumor cell growth. *N Biotechnol.* **30,** 205-209 (2013).

Borras, L. *et al.* Generic approach for the generation of stable humanized single-chain Fv fragments from rabbit monoclonal antibodies. *J. Biol. Chem.* **285,** 9054–9066 (2010).

Burton, R. E., Hunt, J. A., Fierke, C. A., Oas, T. G. Novel disulfide engineering in human carbonic anhydrase II using the PAIRWISE side-chain geometry database. *Protein Sci.* **9,** 776–785 (2000).

Carpenter, J. F. *et al.* Overlooking subvisible particles in therapeutic protein products: gaps that may compromise product quality. *J. Pharm. Sci.* **98,** 1201–1205 (2009).

Chakravarty, R., Goel, S., Cai, W. Nanobody: The "magic bullet" for molecular imaging? *Theranostics* **4,** 386-398 (2014).

Chi, E. Y., Krishnan, S., Kendrick, B. S., Chang, B. S. Roles of conformational stability and colloidal stability in the aggregation of recombinant human granulocyte colony-stimulating factor. *Protein Sci.* **12,** 903–913 (2003).

Correa, A. & Oppezzo, P. Overcoming the solubility problem in *E. coli*: available approaches for recombinant protein production. *Methods Mol. Biol.* **1258,** 27–44 (2015).

Davies, J. & Riechmann, L. 'Camelising' human antibody fragments: NMR studies on VH domains. *FEBS Lett.* **339,** 285–290 (1994).

Day, L. A. & Wiseman, R.L. A comparison of DNA packaging in the virions of fd, Xf, and Pf1. *The Single-Stranded DNA Phages*, 605-625 (1978).

Deng, C. *et al.* Novel recombinant immunotoxin of EGFR specific nanobody fused with cucurmosin, construction and antitumor efficiency *in vitro*. *Oncotarget* **8,** 38568-38580 (2017).

Dong, H. *et al.* Hydrophobic effect on the stability and folding of a hyperthermophilic protein. *J. Mol. Biol.* **378,** 264–272 (2008).

Dougherty, D.A. The cation-π interaction. *Acc. Chem. Res.* **46,** 885–893 (2013).

Ferrara, N., Hillan, K. J., Gerber, H.P., Novotny, W. Discovery and development of bevacizumab, an anti-VEGF antibody for treating cancer. *Nat Rev Drug Discov.* **3,** 391-400 (2004).

Flory, P. J. Theory of elastic mechanisms in fibrous proteins. *J. Am. Chem. Soc.* **78,** 5222–5235 (1956).

Garcin, G. *et al.* High efficiency cell-specific targeting of cytokine activity. *Nat Commun.* **5,** doi: 10.1038/ncomms4016. (2014).

Greenberg, A. S. *et al.* A new antigen receptor gene family that undergoes rearrangement and extensive somatic diversification in sharks. *Nature* **374,** 168–173 (1995).

Hagihara, Y., Mine, S., Uegaki, K. Stabilization of an immunoglobulin fold domain by an engineered disulfide bond at the buried hydrophobic region. *J. Biol. Chem.* **282,** 36489–36495 (2007).

Hamers-Casterman, C. *et al.* Naturally occurring antibodies devoid of light chains. *Nature* **363,** 446-448 (1993).

Hawlisch, H., Meyer, A., Bautsch, W., Klos, A., Köhl, J. Guinea pig C3 specific rabbit single chain Fv antibodies from bone marrow, spleen and blood derived phage libraries. *J. Immunol. Methods* **236,** 117–131 (2000).

Heukers, R. *et al.* Targeting hepatocyte growth factor receptor (Met) positive tumor cells using internalizing nanobody-decorated albumin nanoparticles. *Biomaterials* **35,** 601-610 (2014).

Hussack, G., Hirama, T., Ding, W., Mackenzie, R, Tanha, J. Engineered single-domain antibodies with high protease resistance and thermal stability. *PLoS One* **6,** e28218 (2011).

Hussack, G. *et al.* A V(L) single-domain antibody library shows a high-propensity to yield non-aggregating binders. *Protein Eng. Des. Sel.* **25,** 313–318 (2012).

Holt, L. J. *et al.* Anti-serum albumin domain antibodies for extending the half-lives of short lived drugs. *Protein Eng. Des. Sel.* **21,** 283–288 (2008).

Heldt, C.L., Zahid, A., Vijayaragavan, K.S., Mi, X. Experimental and computational surface hydrophobicity analysis of a non-enveloped virus and proteins. *Colloids Surf. B Biointerfaces* **153,** 77–84 (2017).

Jackson, S. E., Moracci, M., elMasry, N., Johnson, C. M., Fersht, A. R. Effect of cavity-creating mutations in the hydrophobic core of chymotrypsin inhibitor 2. *Biochemistry* **32,** 11259–11269 (1993).

Jäger, M. & Plückthun, A. Domain interactions in antibody Fv and scFv fragments: effects on unfolding kinetics and equilibria. *FEBS Lett.* **462,** 307–312 (1999).

Jespers, L., Schon, O., James, L. C., Veprintsev, D., Winter, G. Crystal structure of HEL4, a soluble, refoldable human V(H) single domain with a germ-line scaffold. *J. Mol. Biol.* **337,** 893–903 (2004).

Kabat, E. A., Wu, T. T., Reid-Miller, M., Perry, H. M., Gottesman, K. S. *Sequences of Proteins of Immunological Interest* (DHHS, 1991).

Kellis, J. T. Jr., Nyberg, K., Fersht, A. R. Energetics of complementary side-chain packing in a protein hydrophobic core. *Biochemistry* **28,** 4914–4922 (1989).

Kodangattil, S. *et al.* The functional repertoire of rabbit antibodies and antibody discovery via next-generation sequencing. *MAbs* **6,** 628–636 (2014).

Köhler, G. & Milstein, C. Continuous cultures of fused cells secreting antibody of predefined specificity. *Nature* **256**, 495-497 (1975).

Ko, J. H. *et al.* Enhancement of thermostability and catalytic efficiency of AprP, an alkaline protease from *Pseudomonas* sp., by the introduction of a disulfide bond. *Biochem. Biophys. Res. Commun.* **221,** 631–635 (1996).

Lammens, A. *et al.* Crystal structure of human TWEAK in complex with the Fab fragment of a neutralizing antibody reveals insights into receptor binding. *PLoS One* **8,** e62697 (2013).

Landry, J. P., Ke, Y., Yu, G.L., Zhu, X. D. Measuring affinity constants of 1450 monoclonal antibodies to peptide targets with a microarray-based label-free assay platform. *J Immunol Methods.* **417,** 86-96 (2015).

Lavinder, J. J., Hoi, K. H., Reddy, S. T., Wine, Y., Georgiou, G. Systematic characterization and comparative analysis of the rabbit immunoglobulin repertoire. *PLoS One* **9,** e101322 (2014).

Lefranc, M. P. Unique database numbering system for immunogenetic analysis. *Immunol Today* **18,** 509 (1997).

Lewis, S. M. *et al.* Generation of bispecific IgG antibodies by structure-based design of an orthogonal Fab interface. *Nat Biotechnol.* **32,** 191-198 (2014).

Li, T. *et al.* Immuno-targeting the multifunctional CD38 using nanobody. Sci Rep. 6, doi: 10.1038/srep27055. (2016).

Li, Y., Cockburn, W., Kilpatrick, J. B., Whitelam, G. C. High affinity scFvs from a single rabbit immunized with multiple haptens. *Biochem. Biophys. Res. Commun.* **268,** 398–404 (2000).

Lin, S. H., Konishi, Y., Denton, M. E., Scheraga, H. A. Influence of an extrinsic cross-link on the folding pathway of ribonuclease A. Conformational and thermodynamic analysis of cross- linked (lysine7-lysine41)-ribonuclease a. *Biochemistry* **23,** 5504–5512 (1984).

Liggins, J. R., Lo, T. P., Brayer, G. D., Nall, B. T. Thermal stability of hydrophobic heme pocket variants of oxidized cytochrome c. *Protein Sci.* **8,** 2645–2654 (1999).

Makvandi-Nejad, S., Sheedy, C., Veldhuis, L., Richard, G., Hall, J. C. Selection of single chain variable fragment (scFv) antibodies from a hyperimmunized phage display library for the detection of the antibiotic monensin. *J. Immunol. Methods* **360,** 103–118 (2010).

Malia, T. J. *et al.* Structure and specificity of an antibody targeting a proteolytically cleaved IgG hinge. *Proteins* **82,** 1656–1667 (2014).

Mankarious, S. *et al.* The half-lives of IgG subclasses and specific antibodies in patients with primary immunodeficiency who are receiving intravenously administered immunoglobulin. *J Lab Clin Med.* **112**, 634-640 (1988).

Marks, J. D. *et al.* By-passing immunization. Human antibodies from V-gene libraries displayed on phage. *J Mol Biol.* **222,** 581-597 (1991).

Martin, D. F., *et al.* Ranibizumab and bevacizumab for treatment of neovascular age-related macular degeneration: two-year results. *Ophthalmology* **119,** 1388-1398 (2012).

Mårtensson, L. G., Karlsson, M., Carlsson, U. Dramatic stabilization of the native state of human carbonic anhydrase II by an engineered disulfide bond. *Biochemistry* **41,** 15867–15875 (2002).

Mitchinson, C., & Wells, J. A. Protein engineering of disulfide bonds in subtilisin BPN'. *Biochemistry* **28,** 4807–4815 (1989).

Mordenti J *et al.* Comparisons of the intraocular tissue distribution, pharmacokinetics, and safety of 125I-labeled full-length and Fab antibodies in rhesus monkeys following intravitreal administration. *Toxicol Pathol.* **27,** 536-544 (1999).

Ota, C., Noguchi, S., Nagatoishi, S., Tsumoto, K. Assessment of the protein-protein interactions in a highly concentrated antibody solution by using Raman spectroscopy. *Pharm. Res.* **33,** 956–969 (2016).

Pace, C. N., Grimsley, G. R., Thomson, J. A., Barnett, B. J. Conformational stability and activity of ribonuclease TI with zero, one, and two intact disulfide bonds. *J. Biol. Chem.* **263,** 11820–11825 (1988).

Palomo, C. *et al.* Trivalency of a nanobody specific for the human respiratory syncytial virus fusion glycoprotein drastically enhances virus neutralization and impacts escape mutant selection. *Antimicrob Agents Chemother.* **60,** 6498-6509 (2016).

Pan, R. *et al.* Rabbit anti-HIV-1 monoclonal antibodies raised by immunization can mimic the antigen-binding modes of antibodies derived from HIV-1-infected humans. *J Virol.* **87,** 10221–10231 (2013).

Pasche, N. *et al.* Immunocytokines: a novel class of potent armed antibodies. *Drug*

Discov Today **17,** 11-12 (2012).

Perchiacca, J. M., Ladiwala, A. R., Bhattacharya, M., Tessier, P. M. Aggregation-resistant domain antibodies engineered with charged mutations near the edges of the complementarity-determining regions. *Protein Eng. Des. Sel.* **25,** 591–601 (2012).

Perchiacca, J. M., Lee, C. C., Tessier, P. M. Optimal charged mutations in the complementarity determining regions that prevent domain antibody aggregation are dependent on the antibody scaffold. *Protein Eng. Des. Sel.* **27,** 29–39 (2014).

Polakis, P. Antibody drug conjugates for cancer therapy. *Pharmacol Rev.* **68,** 3-19 (2016).

Poland, D. G. & Scheraga, H. A. Statistical mechanics of noncovalent bonds in polyamino acids. VIII. Covalent loops in proteins. *Biopolymers* **3,** 379–399 (1965).

Reading, N. S. & Aust, S. D. Engineering a disulfide bond in recombinant manganese peroxidase results in increased thermostability. *Biotechnol. Prog.* **16,** 326–333 (2000).

Reichert, J. M. Antibodies to watch in 2017. *MAbs* **9,** 167-181 (2017).

Rocco, M. & Byron, O. Computing translational diffusion and sedimentation coefficients: an evaluation of experimental data and programs. *Eur Biophys J* **44,** 417–431 (2015).

Roguska, M. A. *et al.* Humanization of murine monoclonal antibodies through variable domain resurfacing. *Proc Natl Acad Sci USA.* **9,** 969-973 (1994).

Roopenian, D. C. & Akilesh, S. FcRn; the neonatal Fc receptor comes of age. *Nat Rev Immunol.* **7,** 715-725 (2007).

Rossi, S. *et al.* Rabbit monoclonal antibodies: a comparative study between a novel category of immunoreagents and the corresponding mouse monoclonal antibodies. *Am. J. Clin. Pathol.* **124,** 295–302 (2005).

Rouet, R., Dudgeon, K., Christie, M., Langley, D., Christ, D. Fully human VH single

domains that rival the stability and cleft recognition of camelid antibodies. *J. Biol. Chem.* **290,** 11905–11917 (2015).

Röthlisberger, D., Honegger, A., Plückthun, A. Domain interactions in the Fab fragment: a comparative evaluation of the single chain Fv and Fab format engineered with variable domains of different stability. *J. Mol. Biol.* **347,** 773–789 (2005).

Saerens, D., Conrath, K., Govaert, J., Muyldermans, S. Disulfide bond introduction for general stabilization of immunoglobulin heavy-chain variable domains. *J. Mol. Biol.* **377,** 478–488 (2008).

Saxena, A. & Wu, D. Advances in therapeutic Fc engineering-modulation of IgG-associated effector functions and serum half-life. *Front Immunol.* **7,** doi: 10.3389/fimmu.2016.00580 (2016)

Schuck, P. Size-distribution analysis of macromolecules by sedimentation velocity ultracentrifugation and Lamm equation modeling, *Biophys J.* **78,** 1606–1619 (2000).

Sliwkowski, M. X. *et al.* Nonclinical studies addressing the mechanism of action of trastuzumab (Herceptin). *Semin Oncol.* **26,** 60-70 (1999).

Suter, M., Blaser, K., Aeby, P., Crameri, R. Rabbit single domain antibodies specific to protein C expressed in prokaryotes. *Immunol. Lett.* **33,** 53–59 (1992).

Takano, K. *et al.* Contribution of hydrophobic residues to the stability of human lysozyme: calorimetric studies and X-ray structural analysis of the five isoleucine to valine mutants. *J. Mol. Biol.* **254,** 62–76 (1995).

Talelli, M. *et al.* Nanobody-shell functionalized thermosensitive core-crosslinked polymeric micelles for active drug targeting. *J Control Release* **151,** 183-192 (2011).

Talelli, M. *et al.* Intrinsically active nanobody-modified polymeric micelles for tumor-targeted combination therapy. *Biomaterials* **34,** 1255-1260 (2013).

Tamura, T., Terada, T., Tanaka, A. A quantitative analysis and chemical approach for the

reduction of nonspecific binding proteins on affinity resins. *Bioconjug. Chem.* **14,** 1222–1230 (2003).

Tanha, J. *et al.* Improving solubility and refolding efficiency of human V(H)s by a novel mutational approach. *Protein Eng. Des. Sel.* **19,** 503–509 (2006).

To, R. *et al.* Isolation of monomeric human V(H)s by a phage selection. *J. Biol. Chem.* **280,** 41395–41403 (2005).

Toussirot, E. & Wendling, D. The use of TNF-alpha blocking agents in rheumatoid arthritis: an overview. *Expert Opin Pharmacother.* **5,** 581-594 (2004).

Uchiyama, S. *et al.* Thermodynamic assessment of domain-domain interactions and in vitro activities of mesophilic and thermophilic ribosome recycling factors. *Biopolymers* **100,** 366–379 (2013).

Uchiyama, S. Liquid formulation for antibody drugs. *Biochim. Biophys. Acta.* **1844,** 2041–2052 (2014).

Ulrich, H. W. *et al.* The intriguing options of multispecific antibody formats for treatment of cancer. *Cancer Genomics & Proteomics* **10,** 1-18 (2013)

Vaneycken, I. *et al.* Immuno-imaging using nanobodies. *Curr Opin Biotechnol.* **22,** 877-881 (2011).

van der Meel R. *et al.* Tumor-targeted nanobullets: Anti-EGFR nanobody-liposomes loaded with anti-IGF-1R kinase inhibitor for cancer treatment. *J Control Release.* **159,** 281-289 (2012).

Van Roy, M. *et al.* The preclinical pharmacology of the high affinity anti-IL-6R Nanobody® ALX-0061 supports its clinical development in rheumatoid arthritis. *Arthritis Res Ther.* **17,** doi: 10.1186/s13075-015-0651-0. (2015).

Vidarsson, G., Dekkers, G., Rispens, T. IgG subclasses and allotypes: from structure to effector functions. *Front Immunol.* **5,** doi: 10.3389/fimmu.2014.00520. (2014).

Wakarchuk, W. W. *et al.* Thermostabilization of the *Bacillus circulans* xylanase by the introduction of disulfide bonds. *Protein Eng.* **7,** 1379–1386 (1994).

Ward, E. S., Güssow, D., Griffiths, A. D., Jones, P. T., Winter, G. Binding activities of a repertoire of single immunoglobulin variable domains secreted from *Escherichia coli.* *Nature* **341,** 544–546 (1989).

Weiner, G. J. Rituximab: mechanism of action. *Semin Hematol.* **47,** 115-123 (2010).

Wörn, A. & Plückthun, A. Mutual stabilization of VL and VH in single-chain antibody fragments, investigated with mutants engineered for stability. *Biochemistry* **37,** 13120–13127 (1998).

Yu, Y. *et al.* Humanized CD7 nanobody-based immunotoxins exhibit promising anti-T-cell acute lymphoblastic leukemia potential. *Int J Nanomedicine* **12,** 1969-1983 (2017).

Zhou, S. J. *et al.* Strategies for bispecific single chain antibody in cancer immunotherapy. *J Cancer.* **8,** 3689-3696 (2017).

Zielonka, S. *et al.* Structural insights and biomedical potential of IgNAR scaffolds from sharks. *MAbs* **7,** 15–25 (2015).

List of Publications

Shinozaki, N., Hashimoto, R., Fukui, K., Uchiyama, S. Efficient generation of single domain antibodies with high affinities and enhanced thermal stabilities. *Sci. Rep.* **7,** 5794 (2017).

Shinozaki, N., Hashimoto, R., Noda, M., Uchiyama, S. Physicochemical improvement of rabbit derived single-domain antibodies by substitutions with amino acids conserved in camelid antibodies. *J Biosci Bioeng.* **in press,** doi: 10.1016/j.jbiosc.2018.01.006. (2018).